Raised Object on a Planar Surface Stroked Across the Fingerpad: Responses of Cutaneous Mechanoreceptors to Shape and Orientation

R. H. LAMOTTE,[1] R. M. FRIEDMAN,[1] C. LU,[1] P. S. KHALSA,[1] AND M. A. SRINIVASAN[2]
[1]*Department of Anesthesiology, Yale University School of Medicine, New Haven, Connecticut 06510; and* [2]*Department of Mechanical Engineering, Research Laboratory of Electronics, Massachusetts Institute of Technology, Cambridge, Massachusetts 02139*

LaMotte, R. H., R. M. Friedman, C. Lu, P. S. Khalsa, and M. A. Srinivasan. Raised object on a planar surface stroked across the fingerpad: responses of cutaneous mechanoreceptors to shape and orientation. *J. Neurophysiol.* 80: 2446–2466, 1998. The representations of orientation and shape were studied in the responses of cutaneous mechanoreceptors to an isolated, raised object on a planar surface stroked across the fingerpad. The objects were the top portions of a sphere with a 5-mm radius, and two toroids each with a radius of 5 mm along one axis and differing radii of 1 or 3 mm along the orthogonal axis. The velocity and direction of stroking were fixed while the orientation of the object in the horizontal plane was varied. Each object was stroked along a series of laterally shifted, parallel, linear trajectories over the receptive fields of slowly adapting, type I (SA), and rapidly adapting, type I (RA) mechanoreceptive afferents innervating the fingerpad of the monkey. "Spatial event plots" (SEPs) of the occurrence of action potentials, as a function of the location of each object on the receptive field, were interpreted as the responses of a spatially distributed population of fibers. That portion of the plot evoked by the curved object (the SEP_c) provided a representation of the shape and orientation of the two-dimensional outline of the object in the horizontal plane in contact with the skin. For both SAs and RAs, the major vector of the SEP_c, obtained by a principal components analysis, was linearly related to the physical orientation of the major axis of each toroid. The spatial distribution of discharge rates [spatial rate surface profiles (SRSs), after plotting mean instantaneous frequency versus spatial locus within the SEP_c] represented object shape in a third dimension, normal to the skin surface. The shape of the SA SRSs, well fitted by Gaussian equations, better represented object shape than that of the RA SRSs. A cross-sectional profile along the minor axis [spatial rate profile (SRP)] was approximately triangular for SAs. After normalization for differences in peak height, the falling slopes of the SA SRPs increased, and the base widths decreased with curvature of the object's minor axis. These curvature-related differences in slopes and widths were invariant with changes in object orientation. It is hypothesized that circularity in object shape is coded by the constancy of slopes of SA SRPs between peak and base and that the constancy of differences in the widths and falling slopes evoked by different raised objects encodes, respectively, the differences in their sizes and shapes regardless of differences in their orientation on the skin.

INTRODUCTION

The shape of an object is an intrinsic physical property that remains invariant with changes in orientation and translation in three-dimensional space. Within a smooth area, that has no edges or tears on the objects surface, the local shape at a point is completely defined by the curvatures and orientations of two orthogonal principal axes. For convex objects, both the principal curvatures are positive. In this paper, we investigate how cutaneous mechanoreceptors encode the orientation and shape of raised toroidal objects on a planar surface. Shape can be defined as the distribution of curvatures at any given point on the object's surface where the local curvature at that point is the reciprocal of the radius of a circle that can be fitted on a given cross-sectional surface profile of the object (Srinivasan and LaMotte 1991).

It is common experience that when the skin is moved over the surface of an object, the shape and orientation of the object are independently tactually perceived even in the face of considerable changes in the contact force or the direction and velocity of movement. It therefore seems reasonable to hypothesize that the responses of cutaneous mechanoreceptors contain information about object curvature and orientation that remains relatively invariant and independent of that related to the parameters of stimulus presentation.

There is ample evidence that cutaneous mechanoreceptors code tactile signals related to object curvature. The responses of slowly adapting, type I and rapidly adapting, type I mechanoreceptive afferents (SAs and RAs, respectively) to small, stepped shaped objects pressed onto or stroked across the fingerpad demonstrated that SAs were exquisitely sensitive to the amount and rate of change in the curvature of the skin and that their responses were modulated by differences in curvature in the vertical plane, for objects both statically indented into or stroked across the skin (LaMotte and Srinivasan 1987a,b; Srinivasan and LaMotte 1987). RAs were predominantly sensitive to the indentation velocity and the rate of change in skin curvature, but only when the objects were stroked across the skin at a sufficiently high velocity. These observations were extended in studies of SA and RA responses to cylindrical bars (LaMotte and Srinivasan 1993; Srinivasan and LaMotte 1991), spheres (Goodwin et al. 1995), and toroids (Khalsa et al. 1998) statically indented into the skin and wavy surfaces, consisting of alternating convex and concave cylindrical bars of differing radii of curvature, stroked across the skin (LaMotte and Srinivasan 1996). It was generally concluded that the size and shape of an object are best represented by the size and shape of the spatially distributed pattern of peripheral neural discharge rates, particularly among the SA population.

The studies of curvature coding in a third dimension, orthogonal to the surface of the skin, have used either two-dimensional structures, such as objects with variations in height with distance along a single axis indented or stroked across the skin (e.g., LaMotte and Srinivasan 1996) or spheres

(Goodwin et al. 1995) and toroids (Khalsa et al. 1998) that were indented but not stroked. In contrast, there are many studies of the peripheral neural coding of spatial pattern and roughness that employed scanned planar surfaces containing two-dimensional raised elements (Connor et al. 1990; Connor and Johnson 1992; Johnson and Lamb 1981; LaMotte and Whitehouse 1986). These have focused primarily on the coding of spatial variations in the horizontal plane using raised elements with flat tops and sharp edges. Little is known of the neural coding of the orientation of single raised elements in the horizontal plane nor of the coding of the three-dimensional objects of such raised structures, of millimeter length scale, stroked across the skin, aside from preliminary observations (LaMotte et al. 1994, 1996).

In the present experiments, we studied the peripheral neural coding of the shape and orientation of a single, three-dimensional raised object on a planar surface that was stroked across the fingerpad. Three object shapes were used, two toroidal and one spherical. For each object, the curvature along one principal axis was the same, whereas the curvature along the orthogonal axis differed. For each object, the indentation force, stroke velocity, and direction of stroking was held constant, whereas the orientation of the object in the horizontal plane was varied.

METHODS

Construction of raised objects of differing shape

Small, three-dimensional objects of differing shape were constructed and mounted on the center of a flat plate having a diameter of 25 mm (Fig. 1*A*). The objects were the top portions of a sphere with a 5-mm radius, and two toroids each with a radius of 5 mm along one axis and differing radii of 1 or 3 mm along the orthogonal axis. Their curvatures (inverse of radii) were 200, 333, and 1,000 m^{-1}. Each object and the plate on which it was mounted (Fig. 1*A*, *right*) were machined from clear, hard acrylic, were transparent, and had smooth surfaces. The flat plate allowed us to differentiate the neural response due the curvature of the objects from that due to a flat surface with no curvature. The heights of the objects ranged from 0.42 to 0.44 mm. At the base of the toroidal objects, the lengths of the major axes were 4.1 and 4.2 mm; the widths of the minor axes were 1.6 and 2.6 mm for the 1 × 5 and 3 × 5 mm toroids. The width of the base of the sphere was 4.3 mm in all directions.

Psychophysical testing with human subjects

A two-interval, two-alternative forced choice procedure was used to determine the discriminability of the shapes or orientations of the stimulus objects, for three human observers. Discriminations of shape and orientation were measured under conditions of *active touch*, wherein the subject actively stroked the object in a natural way. The stimulus object was placed on a raised circular platform (6 in. diam) in a slightly recessed position so that the edge of the planar surface on which the toroid or sphere was mounted rested flush with the surrounding surface of the platform. The subject's arm was supported so that the index finger was poised comfortably above the left side of the stimulus object before each stimulus presentation. At the start of each trial, the subject brought the finger down, approximately at a 25° angle to contact the platform. Using the fingerpad, a single stroke from left to right was made along a linear trajectory of 5 cm at a velocity of ~10 mm/s. The objects were presented in randomly determined order.

During shape discrimination, the subjects stated which of the two objects was less spherical than the other. For each set of 24 trials, the objects (mm radii) were 1 × 5 versus 3 × 5, or 3 × 5 versus 5 × 5. The orientation of the major axis of each toroid was fixed during the set of trials at either 90 or 0° with respect to the major axis of the finger. During orientation discrimination, either the 1 × 5 or the 3 × 5 mm toroid was presented at one of two orientations, in randomly determined order, on each of 24 trials. The orientation pairs were 0 versus 30°, 30 versus 60°, and 60 versus 90°. The orientation of the object was produced by manually rotating the platform. The subject stated which of the two orientations was closer to the orientation of the finger, i.e., closer to 90°. The subjects had no visual cues and verbal feedback as to their performance. Threshold discrimination was defined as 75% correct.

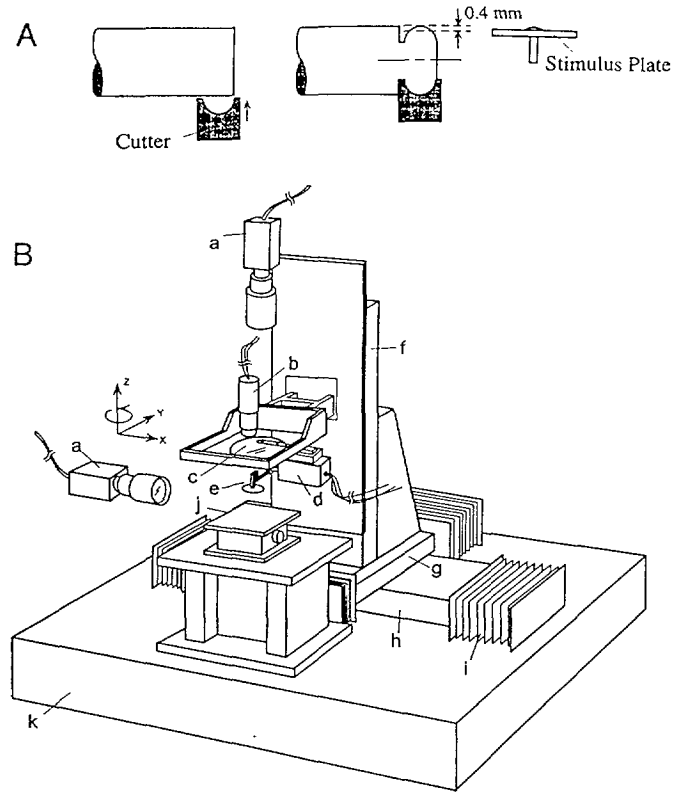

FIG. 1. Procedures for constructing the stimulus object and for controlling its position and contact force as it was stroked over the fingerpad. *A*: a radius cutting tool was used to cut the toroid or sphere from a rotating cylinder. Then, with the axis of the object horizontal, the top was cutoff along a section parallel to the axis, ~0.4 mm from the peak. The resulting form, which, for each toroid had the shape of the top of an egg, was mounted on a flat plate (the "stimulus plate") shown at *right*. The curvatures for the 3 stimulus objects were identical along one axis but differed for the orthogonal axis. *B*: schematic of the tactile stimulator used to control the position and contact force of the stimulus object on the fingerpad. A stimulus plate (*A*, *right*) containing one of the objects was mounted, via its stem, to a lever, containing a 3-axis load cell and attached to a torque motor (Fig. 2*A* for expanded view that includes the finger). The motor was mounted on a 3-axis translation table that was used to control the motion of the stimulus object along a linear trajectory in the horizontal plane while the torque motor controlled the compressional force of the object against the skin. Video cameras (a) provided top and side views of stimulus object on the fingerpad (not shown). A stepper motor (b) rotated a transparent plate (c) to which the torque motor (d) was mounted by a bracket so that the stimulus object (e) could be rotated about its center before applying it to the fingerpad. The platform containing the rotary transparent plate (c) was attached to the *z*-axis (vertical) translator (f), which was mounted in turn to the *y*-axis translator (g) and the latter to the *x*-axis (h) translator. The translation system was bolted to a granite table (k). Dust covers (i) protected portions of the translation mechanisms for *x* and *y*. An adjustable platform (j) was used to support the subject's hand (not shown).

Orientation discrimination was also measured using *passive touch*. Two of the three subjects tested were participants in the active tactile discriminations, whereas the third was tested only on the passive task. The subject's hand rested in a supine position with the middle finger angled upward by ~25° with respect to the horizontal plane. The finger was held against a Plexiglas holder by a post that was glued to the fingernail. The tactile stimulator (Fig. 1*B*) controlled the movement of the object over the subject's fingerpad under parameters of stimulation identical to those used in the neurophysiological experiments. The stimulus object was held up and off the fingerpad by the torque motor before each stimulus application and rotated to a desired orientation. Each stimulus was applied by dropping the stimulus plate onto the fingerpad as the plate was moving, at 10 mm/s, from left to right (0°, i.e., orthogonal to the long axis of the finger). The plate was in contact with the skin during 6 mm of the 10-mm stroke trajectory. The plate was pulled off the skin just before the end of the stroke. The object was then rotated first to a home position and then to a new orientation. The locus of contact with the fingerpad was approximately one-third the distance from the tip of the finger and the crease at the interphalangeal joint. The compressional force was maintained at 15 g (147 mN). There were no visual or auditory cues.

Method of applying objects to the skin during neurophysiological experiments

The hand was restrained, palm-up, in plasticine with the stimulated finger typically angled upward by ~25° with respect to the horizontal plane. A post was glued to the fingernail and sunk into the plasticine to maintain the position of the finger during tactile stimulation. A vertical post, mounted to the back of the plate containing the raised object (Fig. 1*A, right*), was inserted into the end of a lever containing strain gauges (Brock Research, Newton, MA) that allowed independent measurements of contact force on three axes (Fig. 2). The lever was mounted to a torque motor (Cambridge Technology, Watertown, MA) that maintained compressional force between the object and the skin at 15 ± 0.5 g during stroking (Fig. 2). The torque motor was mounted to a rotary platform that could change the orientation of the object within the horizontal plane (Fig. 1*B*). The platform was mounted to a three-axis, servo-controlled translation table (Anorad, Hauphaug, NY) that was used to stroke the object over the skin in the horizontal plane (X, Y) and make adjustments of the vertical position (Z) of the torque motor at the beginning of an experiment. The orientation of the stroke trajectories was orthogonal to the long axis of the finger and defined as 0°. The position, velocity, and acceleration for the four axes (X, Y, Z, and rotation) were under program control of a dedicated microprocessor (digital axis controller; Anorad) with positional resolution better than a micrometer. Before stroking, the object was rotated to the desired orientation and then stroked, forward and backward (x-axis in Fig. 1*B*), along a series of laterally shifted, parallel, linear trajectories over the fingerpad. Lateral shifts of the trajectories (y-axis in Fig. 1*B*) were either 0.1 mm, for the majority of fibers tested, or 0.2 mm. Trajectory lengths ranged from 6.0 to 10.0 mm. The areas encompassed by the stroking were always square. Thus a 6.0 × 6.0 mm area, centered on the fiber's receptive field, would be stimulated by having a trajectory length of 6.0 mm and 60 lateral shifts of 0.1 mm (a total of 120 strokes, 60 forward and 60 backward). The velocity of stroking was 10 mm/s. The orientation of the objects relative to the trajectory of stroking was varied from 0, 30, 60, and 90°.

Surgical preparation

Experiments were performed on anesthetized monkeys (*Macaca fasicularis*, $n = 9$) as has been described previously (e.g., LaMotte and Srinivasan 1987a). Briefly, an animal was sedated with ketamine hydrochloride (10 mg/kg im), and deep anesthesia (areflexic to painful cutaneous pinch but spontaneously breathing) was maintained with supplemental pentobarbital sodium (35 mg/kg iv). The animal was warmed to maintain body temperature (96 ± 2°F), and hydrated with lactated Ringer solution (100 ml/h). The elbow was clamped and the hand secured palm up. Short pegs were glued to the fingernails, and the dorsal aspect of the fingers were pressed into plasticine. Molding the plasticine around the fingers secured them so that they would not move during the subsequent mechanical stimuli. The median or ulnar nerve in the upper or lower arm, innervating the digits of a hand, was surgically exposed using sterile technique. Skin flaps were used to hold a pool of mineral oil covering the exposed nerve. Neural recordings were made from microdissected filaments of fascicles in the exposed nerve. At the end of the experiment, the mineral oil was removed and the incision site thoroughly cleansed. Muscle and facial layers were sutured in sequence, and the skin was sutured closed. Anesthesia was discontinued, and the animal was allowed to awake normally. Antibiotics to prevent infection were given starting 24 h before the experiment, and twice daily for 1 wk after the experiment and longer if any signs of infection were present. A minimum of 3 wk occurred between subsequent experiments. In total, an animal could have received up to eight experiments on the upper and lower, median and ulnar nerves in the left and right arms. On the final experiment, the animal was killed by overdose of anesthetic.

Electrophysiological recordings

Mechanically sensitive afferents were sought whose receptive fields (RFs) were centrally located on the fingerpads of digits 2–4. The evoked neural responses were amplified (5K) and band-pass filtered (30–3,000 Hz). The neural responses of single afferents were isolated using a window discriminator. With the use of standard criteria, afferents were classified as either slowly (type I) or rapidly adapting (type I) afferents (SAs or RAs, respectively). In studies of shape coding, responses were recorded from 16 SAs and 11 RAs to objects of differing curvature and, for the toroids, a constant orientation of 90°. In studies of orientation coding, responses were recorded from a subset of these afferents, six SAs and five RAs, to different orientations of each two toroids and to a single orientation of the sphere.

Von Frey type nylon filaments (19, 50, and 69 mN; Stoelting, Chicago, IL) were used to map the border of the RF under ×20 magnification using a video camera mounted on a dissecting microscope. Although the angle of elevation of the finger was approximately the same in each experiment and the RFs of the fibers located on the volar surface of the fingerpad, minor variations in the position of the finger were needed from one fiber to the next. These were required so that the most sensitive spot, defined as the location in the RF with the lowest response threshold, would lie directly beneath the center of the stimulus object. The response threshold was defined as the minimal force necessary to elicit a single action potential, under nylon filament stimulation. The RF map was drawn, relative to the fingerpad, on clear acetate mounted on the screen of a video monitor.

Data collection

The sampling rates for all data collection were performed at 1 kHz. Indentation force and position were acquired from analog outputs from the indentation torque motor. The planar position of the stimulus was acquired from the digital axis controller. The time of occurrence of each action potential was acquired from the window discriminator. All data were displayed in real time by a computer and stored for subsequent analysis.

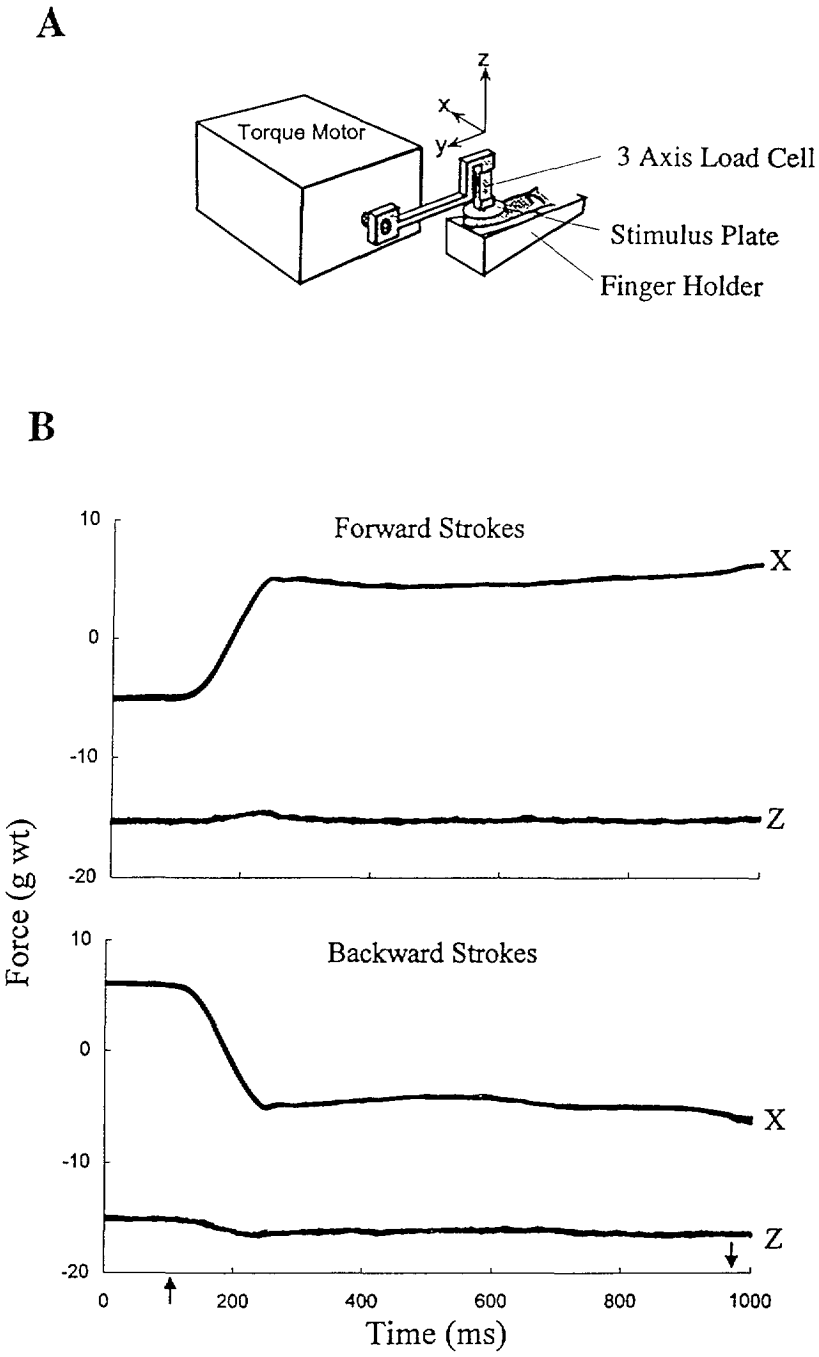

FIG. 2. Methods of force control and measurement with examples of typical force traces recorded when stroking the stimulus plate across the fingerpad. *A*: method of force control and measurement. The stimulus plate was mounted to a lever arm containing a 3-axis load cell that was used to obtain independent measurements of force along each axis (x, y, and z). Small changes in angular displacement of the lever arm produced by a torque motor (mounted to a translation table as shown in Fig. 1*B*) maintained the compressional force (z) constant as the stimulus plate was stroked across the fingerpad. A post was glued to the fingernail to hold the back of the finger against a Plexiglas holder (humans) or plasticine (monkeys). The stimulus plate, to which the stimulus object was mounted, was inscribed with marks (not shown) that allowed accurate orientation of the object in the horizontal plane and its alignment with the fiber's receptive field before stroking. *B*: superimposed force traces on each axis. These traces were obtained as the 1 × 5 mm toroid, oriented 90°, was stroked 6 times in each direction (forward and backward) along the same trajectory, parallel to the x-axis (0° orientation). Upward and downward arrows, respectively, indicate the beginning and end of stroking. Before the 1st stroke, the stimulus plate indented the center of the fingerpad and was then moved leftward to the start location of the forward stroke, resulting in an initial force on the x-axis of ~5 g.

)ata analysis of the neural representation of the wo-dimensional outline of an object's shape in the orizontal plane

Each object was stroked from left to right and then from right to ft along a series of parallel trajectories orthogonal to the long axis f the finger in the horizontal plane. The sequences of nerve impulses enerated in response to each stroke, while collected as a temporal equence, were plotted as spatial events and thus formed a "spatial vent plot" (SEP) (Johnson and Lamb 1981; Johnson and Hsaio 992). An SEP obtained from strokes in a single direction was nterpreted as indicating how a spatially distributed population of echanoreceptors would respond to the two-dimensional outline of ie object's shape in the horizontal plane, parallel to the surface of the skin. In the example shown in Fig. 3*A*, the object was stroked along each trajectory beginning with the flat plate on the left side of the figure and ended with the flat surface at the extreme right. To view the same events as a series of temporal sequences, the origin of time for each stroke would be at the left and the time scale obtained by dividing the distance by the stroke velocity (10 mm/s). A pattern of impulses generated by a given stroke can be viewed as a spatial sequence in two ways. If one imagines that the skin of the fingerpad moves at the given stroke velocity over the stationary object, each dot in the figure would represent the horizontal location of the center of a fiber's receptive field on the object's surface each time a nerve impulse occurred as the skin moved from left to right over the object. An alternative view, and the one we presently adopt, is to interpret the pattern of impulses (dots) as representing a snap-

shot of the instantaneous response of a hypothetical population of mechanoreceptors with identical neural and biomechanical response properties and spatially distributed over the fingerpad. The snapshot occurs at the moment in time when the object has reached a central location on the fingerpad along the stroke trajectory.

An SEP that represented the response to the curved object and not to the surrounding flat plate, "SEP_c" (Fig. 3*A*, *right*) was obtained in the following manner. Each dot in the SEP was assigned an instantaneous frequency (IF), defined as the inverse of the distance (in mm) between sequential action potentials along a given stroke. The actual value used was the average of the IF calculated using the action potential before and the IF calculated using the one after a given action potential. Taking the average of these two values effectively served to make the outline and thus the shape of the SEP more apparent. Next, the mean peak IF was sought in the central 4 × 4 mm area of the SEP. This area typically encompassed most if not all of the response

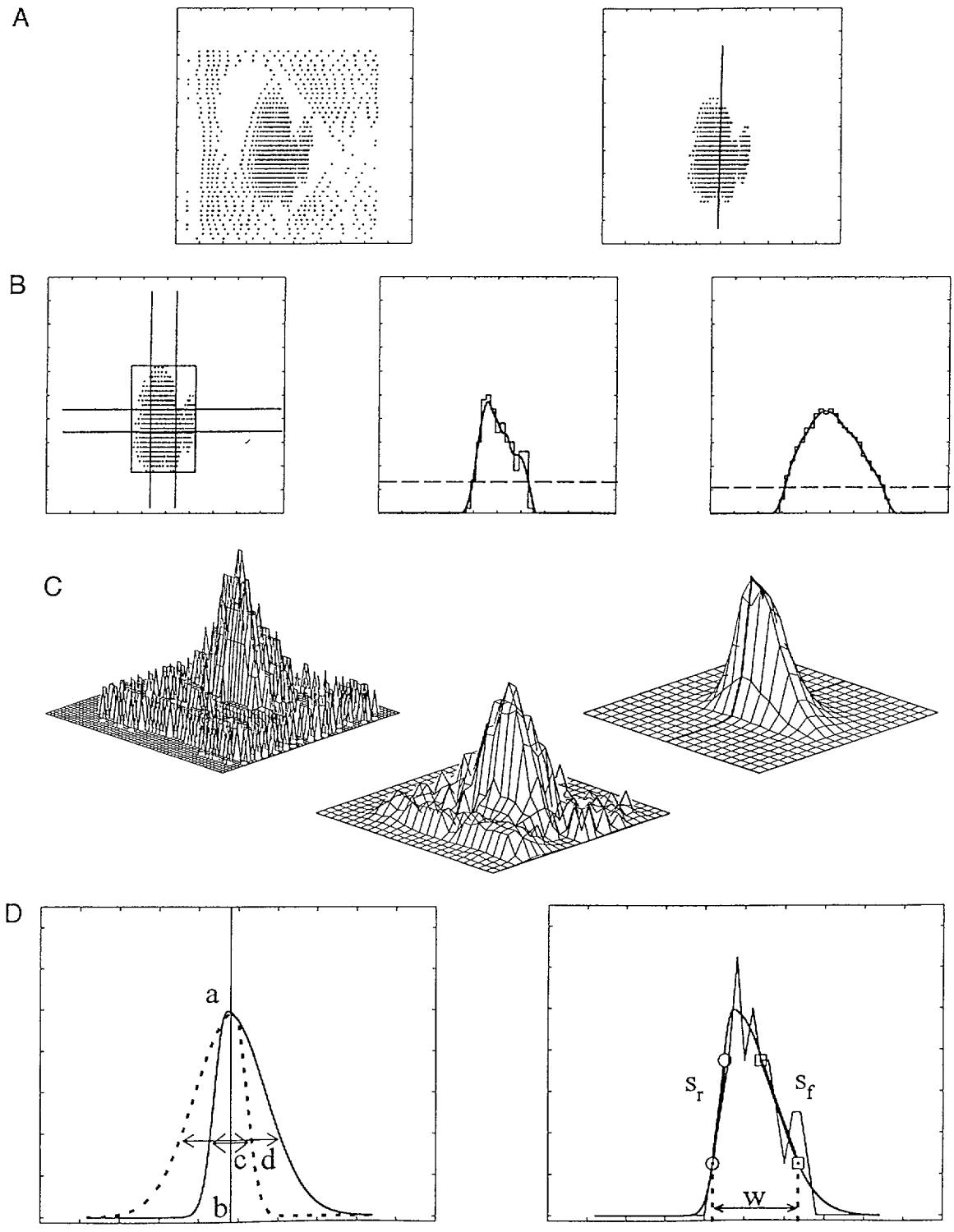

) the raised object. The mean peak IF was defined as the average of ıe IFs within the top 5%, i.e., 95–100 percentile, of all the IFs in the entral area. This process found the mean peak while eliminating xtreme, outlying values. Next, all dots in the SEP with IFs that were :20% of the mean peak IF were eliminated. The threshold of 20% ıas chosen because it was found that 95% of IFs due to stimulation y the flat plate were less than this value. Finally, any remaining dots ı the SEP with IFs that were peripheral to the now delineated region ı response were discarded, resulting in the SEP_c.

In addition to producing SEP_cs of the responses of individual bers, composite SEP_cs were also made by combining the re- ponses of the same fiber type (SA or RA) to a particular object ı given shape and orientation. For each of these composites, the ıw data were pooled by aligning, by eye, the centers of the areas f responses of the individual SEP_cs. The pooled raw data were ıen processed in the identical fashion as described below for the EP_cs from individual fibers.

)ata analysis of the neural representation of an object's ientation

A measure of the neural representation of the orientation of the)ject in the horizontal plane was obtained by using a principal)mponents analysis (Morrison 1967) to determine the orientation the cluster of dots in each individual SEP_c (Fig. 3*A, right*) and ıch composite SEP_c. This analysis determined the orientation of .e vector that minimized the squared distances between it and the)sitions of the dots in the cluster.

)ata analyses of the neural representation of the third ·nension of an object's shape, orthogonal to the surface the skin

Two methods were used to analyze the neural coding of an)ject's shape in the vertical plane based on the spatial distributions fiber discharge rates. The first method analyzed a fiber's spatial te profile (SRP) defined as discharge rate (impulses/s) plotted a function of distance along a line centrally located within the EP_c and parallel to the minor or the major axis of a toroid oriented 90°. An SEP_c obtained in response to an object whose orientation ·viated from 90° was first rotated by an amount equal to the viation. A rectangle was formed with sides that bordered the ıreme edges of the SEP_c (Fig. 3*B, left*). Two strips, each 1 mm wide and forming a cross, were centered within the rectangle. The mean IF was determined for successive bins of 0.2 × 1.0 mm in increments of 0.2 mm along the strip. For any given SEP, the SRPs evaluated the profiles of response to the major and minor axes of the object. The width of the central strip was chosen to be 1 mm because it represented 50% of the width of the smallest object, the 1 × 5 toroid, during stroking parallel to its major axis. We used this to compare the responses to the central region of curvature, without influences due to the edge of the curvature, between all the objects and all the orientations and trajectories.

The SRP was analyzed by fitting it with an eighth order polynomial. This equation was found to provide the best fit, as determined by eye (Fig. 3*B, middle and right*). Once fitted, this equation was used to determine the following four parameters for each of the SRPs: *1*) peak height, *2*) width, *3*) rising slope, and *4*) falling slope. The width was defined as the length of a horizontal line, located 25% of the distance from the base to the peak height, and extending from its intersection with the left edge of the response profile to its intersection with the right edge. The value of 25% was chosen as the minimal distance from the base that was, for most SRPs, still above the background responses produced by the flat plate. The rising and falling slopes were calculated from lines connecting the peak height and the points of intersection between the response profile and the horizontal line representing the width of the SRP.

The second method of analyzing the neural representation of shape in the vertical plane used spatial discharge rate surfaces (SRSs for "spatial rate surfaces") for determining the three-dimensional form of the SEP_cs. An SRS was developed from each fiber's SEP_c and from composite SEP_cs obtained from the combined responses of SAs or RAs by plotting as a Z coordinate, the mean IF within each areal bin of 0.04 mm^2 for successive bins along the X, Y coordinates (Fig. 3*C, left*). The SRS allowed a qualitative evaluation of how isomorphic the neural response of a population of mechanoreceptors was to the geometry of the object. Surface plots of the raw SRSs were smoothed via "inverse distance interpolation," using Sigma Plot 3.0 software from SPSS (Chicago, IL; Fig. 3*C, middle*). Next, each raw SRS was fitted, as shown in Fig. 3*C, right,* with the following Gaussian surface equation

$$f(x_r) = a \exp(-0.5\{[(x - b)/c]^2\})$$

$$f(x_f) = a \exp(-0.5\{[(x - b)/d]^2\})$$

$$f(y_d) = a \exp(-0.5\{[(y - e)/f]^2\})$$

FIG. 3. Procedures for estimating the representation of object shape and orientation in the responses of a population of ·ers based on the responses of a single fiber. Refer to METHODS for further details. *A, left*: spatial event plot (SEP) of the ponses of a single slowly adapting, type I mechanoreceptive afferent (SA) fiber to the 1 × 5 mm toroid oriented 90° and oked from left to right along a series of parallel trajectories orthogonal to the long axis of the finger in the horizontal plane. ch dot is the location of the center of the toroid when an action potential occurred. After each stroke from left to right the ject was shifted proximal to distal (upward in the figure). The tic mark spacing on the coordinate axes is 1 mm. *A, right*: ered version, (SEP_c), of the SEP in *A* in which dots separated by distances more than a criterion amount, based on tantaneous frequency with respect to the preceding and subsequent dot, have been removed. Solid line is the major vector ermined by a principal components analysis, representing the orientation of the cluster of dots. Left side of the response evoked by the leading edge of the object as it moved from left to right. *B*: determination of the center of the SEP_c and 2 ıtral strips (superimposed on the SEP in the *left panel*) from which spatial rate profiles (SRPs) plotting discharge rate, in ıs of 0.2 × 1.0 mm for successive increments of 0.2 mm along the strip, were derived for the minor and major axes (*middle* l *right panels*, respectively). From the 8th order polynomial fitted to each SRP, response widths (horizontal dashed lines) l average slopes of the rising and falling phases were obtained. *C, left*: mesh plot, from the SEP in *A, left*, of discharge rate ıpulses/s) in areal bins of 0.04 mm^2. *C, middle*. same mesh plot after smoothing by inverse distance interpolation (Sigma)t 3.0 software from SPSS, Chicago, IL). *C, right*: asymmetric Gaussian surface fitted to the mesh plot obtained from the P_c in *A, right*. *D, left*: cross-sectional profile (solid curve) through the center of the asymmetric Gaussian surface along the ıxis at the location indicated by the thick line in *C, right*. The vertical line through the peak amplitude (a) and the center the Gaussian surface (b) indicates that the Gaussian surface was divided into 2 halves along the Y-axis, the left half fitted h one Gaussian equation (solid curve on the *left*, dotted on the *right*) while the right half was fitted with another (solid ve on the *right*, dotted on the *left*). Widths of the 2 Gaussians at 60.7% of the peak height are indicated by c and d. *D, ht*: method used to measure slope. The smooth curve is the same asymmetric Gaussian profile represented by the solid curve .he *left panel*. The rising and falling slopes, S_r and S_f, were determined by linear extrapolation between points (○) that had plitudes of 25 and 75% of the peak. Superimposed histogram represents the discharge rates in bins of 0.2 mm evoked by a gle forward stroke as obtained from a center slice through the mesh plot in *C, left*.

$$f(y_p) = a \exp(-0.5\{[(y - e)/g]^2\})$$

$$\text{If } (x < b) \text{ then } f(x) = f(x_r) \quad \text{otherwise } f(x) = f(x_f)$$

$$\text{If } (y < e) \text{ then } f(y) = f(y_d) \quad \text{otherwise } f(y) = f(y_p)$$

$$z = f(x) * f(y)$$

This equation had several advantages. First, the form of the Gaussian surface equation allowed for asymmetries along a given axis as well as for the orthogonal axis. Second, the parameters of the equation could be directly related to the overall geometry of the SRS. The parameters ($a - g$) of the equation each have direct physical interpretations: a is the peak magnitude of the surface; b and e define the center of the Gaussian surface where it splits into halves along the X and Y axes; c and d define the widths of the rising and falling portions, respectively, of the Gaussian surface at 60.7% of the peak height and parallel to the X axis, respectively (Fig. 3*D, left*); and f and g define the widths of the rising and falling portions, respectively, of the Gaussian surface at 60.7% of the peak height and parallel to the Y axis. The conditional statements after the equations specify that for one axis only, one of the two Gaussian equations for that axis is used when fitting its part of the Gaussian surface. A third advantage is that the fitted Gaussian surface is similar to the general, nonlinear surface previously used by Goodwin et al. (1995) and Khalsa et al. (1998) to fit population responses obtained from peripheral mechanoreceptors. Fitting SRSs with the Gaussian surface equation was accomplished with commercially available software (TableCurve 3D, SPSS, Chicago, IL). Because the RA SRSs were bimodal in form, the Gaussian surface was fitted only to the leading half of the response.

In addition to the form and amplitude parameters of the Gaussian fitted SRS, parameters comparable with the slopes and widths obtained from SRPs were obtained from cross-sectional profiles through normalized Gaussian fitted SRSs. The SRSs for each fiber were normalized to the fiber's greatest peak discharge rate, which was always evoked in response to the 1 × 5 mm toroid (oriented at 90°). Two cross-sectional profiles through the center of each normalized Gaussian fitted SRS were obtained, one parallel to the minor axis of the object (Fig. 3*C, right*) and one parallel to the major axis. The width of each profile was calculated at a height that was 25% of the distance from the base to peak. The rising and falling slopes of each profile were estimated from the primarily linear portion of the Gaussian curve, that is from the slope of a line fitted to points at 25 and 75% from the peak (Fig. 3*D, right*).

Statistical analyses

Assessments of the significance of differences in parameters obtained from the principal components analyses, the SRPs, and the Gaussian surfaces for two or three object shapes, two stroke directions and four object orientations were performed with one- or two-way repeated measures analyses of variance (ANOVAs) or repeated measures ANOVAs on ranks. Post hoc analyses applied the Student-Newman-Keuls pairwise multiple comparison method. All statements referring to statistical significance were based on a probability criterion of $P < 0.05$.

RESULTS

Sensory discriminations of shape and orientation

Under conditions of active touch, each subject performed each discrimination task at levels that were well above the threshold criterion of 75%. For discriminations of shape, the two toroids were discriminated by a mean percentage correct of 98.7 and 84.7 at orientations of 90 and 0°, respectively. The corresponding percentages at the same orientations for the 3 × 5 and 5 × 5 mm objects were 91.7 and 89.0. For discriminations of object orientation, the mean percentages correct for 0 versus 30°, 30 versus 60°, and 60 versus 90° were each >90%. Orientation discrimination under passive touch was virtually identical to that under active touch. The mean percentages correct for 0 versus 30°, 30 versus 60°, and 60 versus 90° were each >90%. Thus human subjects could easily discriminate between the different orientations and shapes of the objects used in the neurophysiological experiments.

Neural coding of orientation

Both the orientation of the raised toroid and the two-dimensional outline of the contact region between the skin and the object were represented in the SEPs of single SA and RA responses. SEPs, evoked in a representative fiber of each type in response to the 1 × 5 mm toroid, are shown in Fig. 4. All strokes were in the "forward" direction (from *left* to *right* in the figure). The SAs often responded to the flat plate with a steady discharge that paused just before the leading edge (left side of the of the dense cluster) and just after the raised object moved over the most sensitive spot in the receptive field (Fig. 4*A*). The RAs typically responded in bimodal fashion to the object in a way that seemed to begin just before the object reached the most sensitive spot followed by a pause and another burst after it passed over this spot (Fig. 4*C*). Also shown, for the RA and SA, are the corresponding SEP_cs after background responses to the plate were removed (Fig. 4, *B* and *D*). The major vector that described the spatial orientation of the cluster of action of action potentials was determined by principal components analysis and is superimposed on each SEP_c. In general, the orientation of the major vector, termed the "response orientation," corresponded to the physical orientation of the shape equally well for SAs and RAs in response to the 1 × 5 mm toroid (Fig. 4).

Responses to the 3 × 5 mm toroid were similarly analyzed. The resultant major vectors were related to physical orientation, although less accurately for SAs at 0° (Fig. 5). These SEPs have wider and rounder shapes than those evoked by the 1 × 5 mm toroid but with each still having in most cases an orientation close to the physical orientation of the object. It is important to note that the orientations of the major vectors in Figs. 4 and 5 were not determined solely by the outlines of the spatial responses to the raised object but are also influenced by the spatial distribution of discharge rates within the response. For example, the responses to 60 and 30° in Fig. 5 have outlines of similar shape yet result in different vector orientations.

To include the individual differences between fibers, and yet obtain a more representative neural image of the population response, the responses of a given fiber type were combined. The SEP_cs for each of the seven SAs tested were superimposed, as were those for the five RAs, for each orientation of each toroid by aligning the centers using the method shown in Fig. 3*B, left*. Each composite SEP_c is shown in Fig. 6 along with its major vector. The orientation of the vector shifted in relation to the physical orientation of each toroid for both the SAs and RAs. Also apparent in these panels is a relationship between the outline of the base of the object and the outline of the SEP_c, which became more circular as the angle between the major vector and the direc-

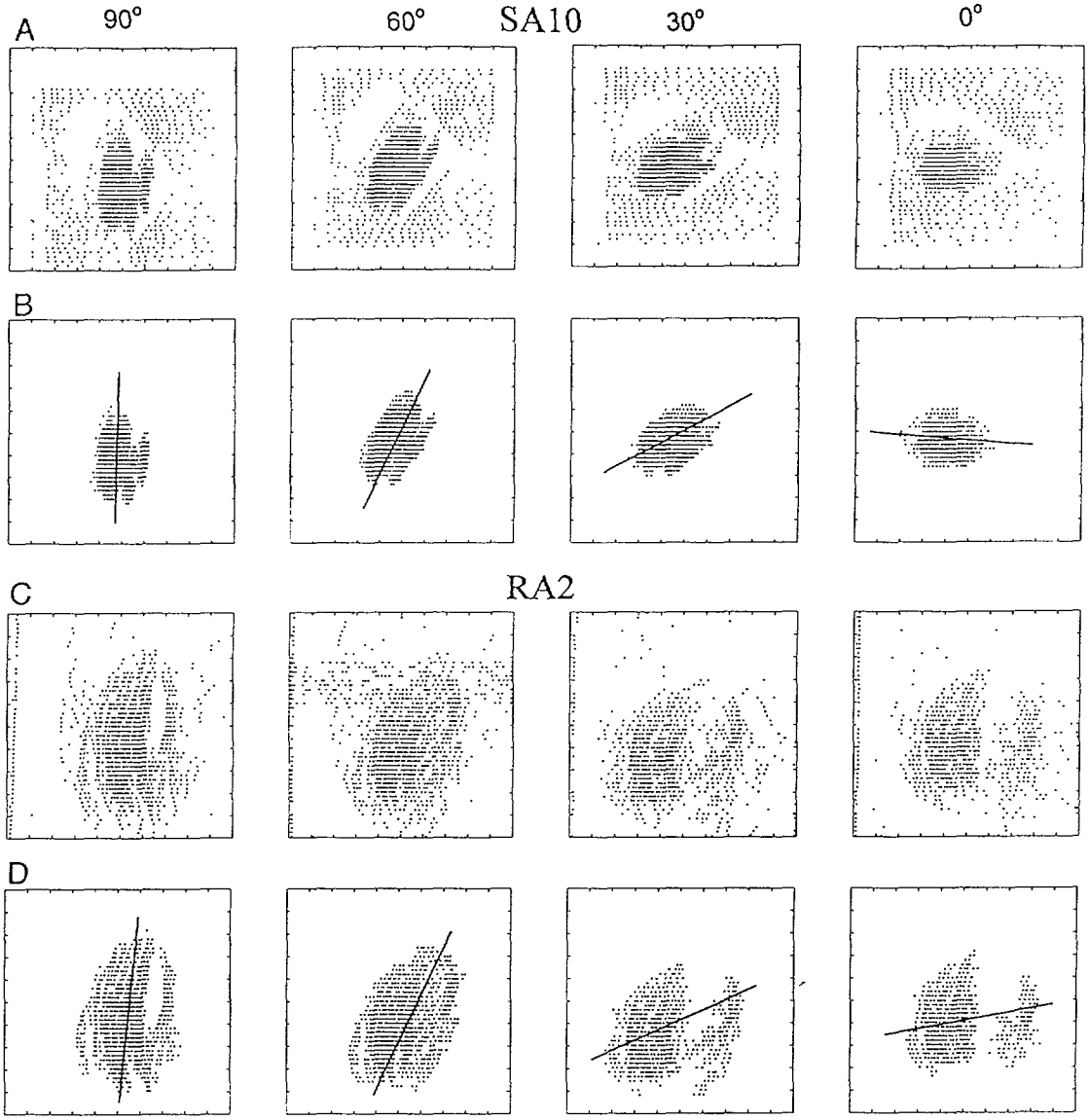

FIG. 4. Spatial event plots of the responses of a single SA and rapidly adapting, type I mechanoreceptive afferent (RA)) different orientations of the toroidally shaped object with 1 × 5 mm radii. The toroid was oriented 90, 60, 30, and 0° to ıe direction of stroking that was from left to right, perpendicular to the long axis of the finger. *A* and *C*: SEPs representing ıw data obtained from an SA and RA. *B* and *D*: filtered versions of same SEPs. Each panel contains an SEP from which ıckground responses to the planar surround have been removed (SEP_c) from the SEP shown directly above and on which superimposed the major vector (solid line) that best describes the spatial orientation of the cluster of action potentials as ɛtermined by a principal components analysis (see Fig. 3*A*). Tic mark spacing on each axis is 1 mm.

on of stroking approached the orientation of zero. The SEP_c RAs was typically larger than that for the SAs. Within ıch SEP_c, the density of activity was highest in the central ɛgion for SAs. In contrast, the density within the central ɛgion of the SEP_c was lowest for the RAs.

All of the data up to this point were obtained from strokes ı a single ("forward") direction. The principal components ıalyses were repeated for the SEP_c data obtained from single bers in response to backward strokes of the same objects and ɛientations. A repeated measures ANOVA was performed on ıe response orientation measures obtained with two fiber pes, four orientations, two toroids, and two stroke directions. here was a significant effect of orientation ($P < 0.05$) for ıch fiber type and each toroid for each direction of stroking. There were no significant differences due to stroke direction nor any significant interactions ($P > 0.1$). For the 1 × 5 mm toroid, every pairwise comparison between orientations was significant for RAs; for the SAs, only 30 versus 0° was not significant. For the 3 × 5 mm toroid, each pairwise discrimination between orientations was significant, except 90 versus 60° and 30 versus 0° for the RAs and 90 versus 60°, 60 versus 30°, and 30 versus 0° for the SHs.

The major vectors obtained from the composite (superimposed) SEP_cs were compared with the mean major vectors obtained from individual fibers, and the orientation of each was plotted against the physical orientation for each toroid (Fig. 7). All the curves for SA and RA fibers indicate that the relationship between the physical and the response orien-

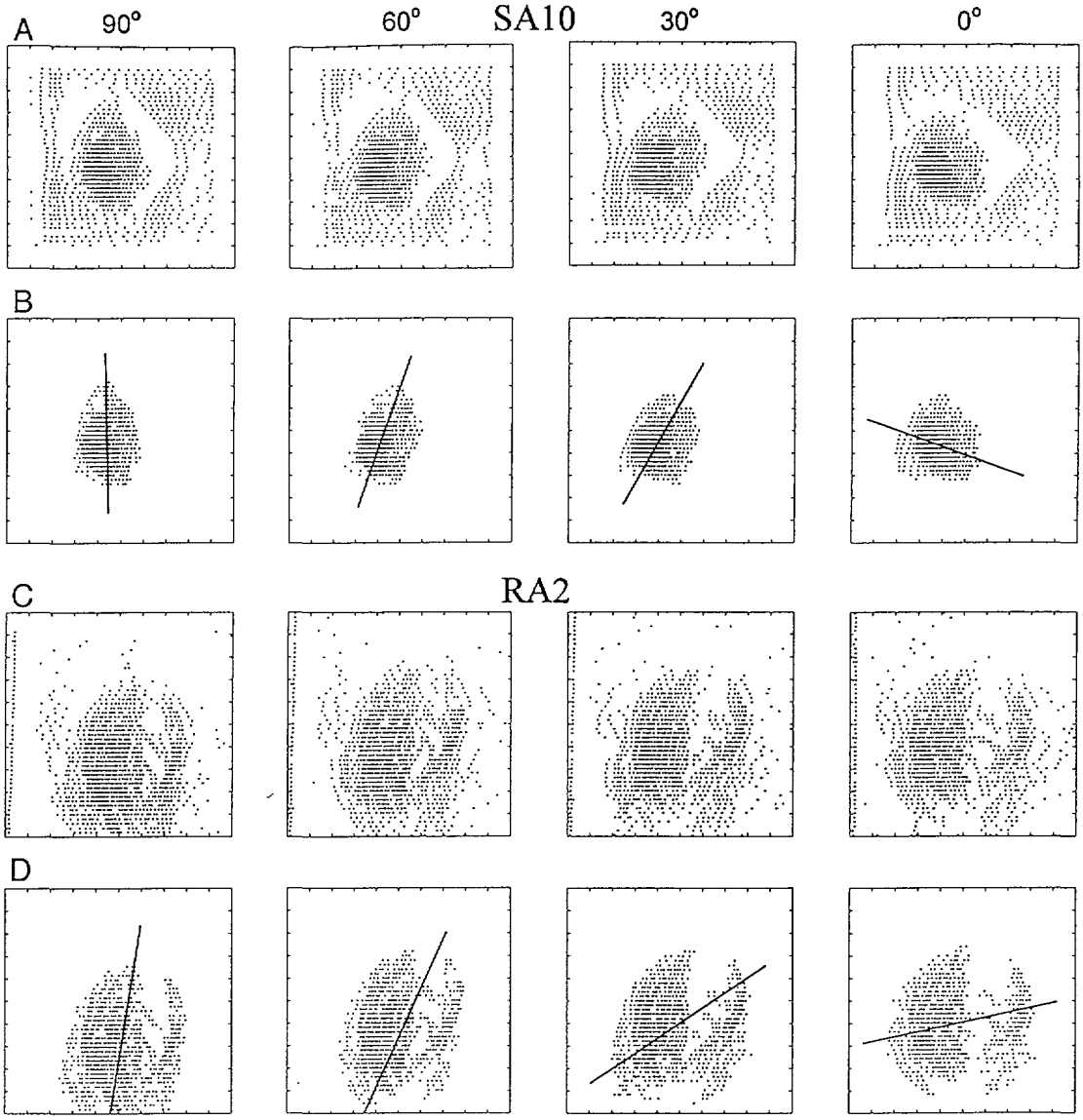

FIG. 5. Spatial event plots of the responses of a single SA and RA fiber to different orientations of the 3 × 5 mm toroid. The SEP_cs and superimposed major vectors were obtained from the same fibers and plotted in the same format as described for Fig. 4. *A* and *B*: responses of the SA. *C* and *D*: responses of the RA.

tations was approximately linear for each object, although the deviation from linearity was greater for the 3 × 5 mm toroid. The R^2 values for the data in SAs and RAs, respectively, were 0.69 and 0.85 for the 1 × 5 and 0.51 and 0.62 for the 3 × 5 mm toroids. The variability in response was clearly greater for the 0 and 30° orientations than for the orientations of 60 and 90°, and greater for the 3 × 5 than the 1 × 5 mm toroid. This was due in part to a decrease in asymmetry in the shape of the SEP_c, accompanying the decreased toroidal curvature in the direction of stroking, for the 0 and 30° as opposed to the 60 and 90° orientations.

Neural coding of shape

NEURAL REPRESENTATIONS OF THE TWO-DIMENSIONAL OUTLINE OF THE OBJECT IN THE HORIZONTAL PLANE. Both the shape and the size of the two-dimensional outline of the raised object in contact with the skin are represented by the borders of activity of each SA and RA. The outline of the base of each object is superimposed on the SEP of the responses of typical SAs and RAs in Fig. 8 to each object and orientation, stroked in the forward direction (from left to right). The area of influence of the raised object on the responses of the RAs, as reflected in their SEPs was generally both wider and longer than the actual length and width of the base of the object and more extensive than on the responses of the SA. A Von Frey type filament (50 mN) was used to measure the widths of the receptive fields orthogonal to the long axis of the finger. A significant positive correlation ($r = 0.61$) was found between the widths of the receptive fields and the widths of the SEP_cs, the latter measured through its middle cross-section, orthogonal to the finger axis for all three raised objects oriented at 90°. The mean widths of the receptive fields were 2.5 mm for the SAs and 3.08 mm for the RAs. This small difference in receptive-field width could not explain the difference in

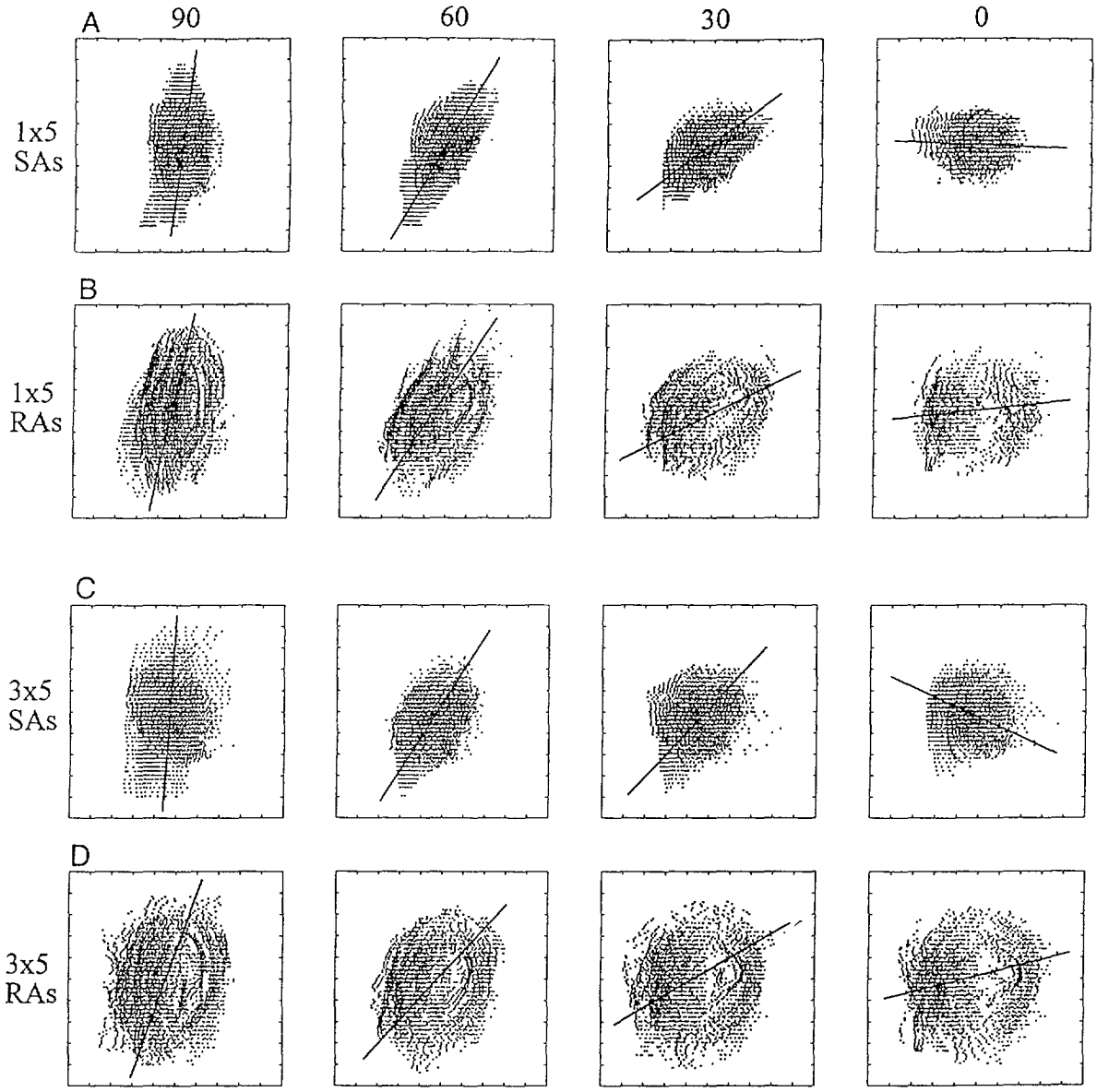

IG. 6. Spatial event plots of the combined responses of a group of SAs and a group of RAs to different orientations of h toroidally shaped object. For each fiber type, the SEP_cs obtained in response to a given orientation of the object, stroked m left to right, were aligned at their geometric centers (Fig. 3*B*, *left panel*) and superimposed. Solid line in each panel he major vector, determined by a principal components analysis. Tic mark spacing on each axis is 1 mm. *A* and *C*: nbined responses of 6 SAs to the toroids, with radii on the minor axis of 1 and 3 mm, respectively, oriented 90, 60, 30, ! 0° to the direction of stroking. *B* and *D*: combined responses of 5 RAs to the same objects and orientations.

dths in the SEP_cs of RAs and SAs. Rather, the greater dths of the RA SEP_cs were due in large part to an earlier ponse onset and to a later offset in response.

As the responses in Fig. 8 were generated by the object ving from left to right, the left side of each SEP represents response to the leading edge of the raised object and the ht side, the trailing edge. The SEPs are arranged in order ncreasing curvature, in the horizontal plane, at the leading ge of the base of each object. For SAs, the shape or curva- e of the left boundary of the response to the object en- led the curved shape of the leading edge of the object in tact with the skin more faithfully, than the shape of the ling edge of the response. This was not always the case RAs, where the reverse was sometimes true. In general, the curvature of the response increased with the increasing curvature of the object in the horizontal plane. The two-dimensional shape of the neural response was typically less clearly defined for RAs than for SAs, possibly due to their greater sensitivity to the vertical velocity of the skin and possibly the local vibratory motions of the skin induced by the passing object. Similarly, the size of the object in contact was better defined by SAs than by RAs. The widths of the RA responses were generally greater than those of the SAs due to an earlier start and later ending of the responses. The major contributing factor to the greater width of RA response was the presence of an "OFF response" to unloading as the object moved away from the most sensitive spot in the receptive field. For the sphere, and toroids oriented at 0°,

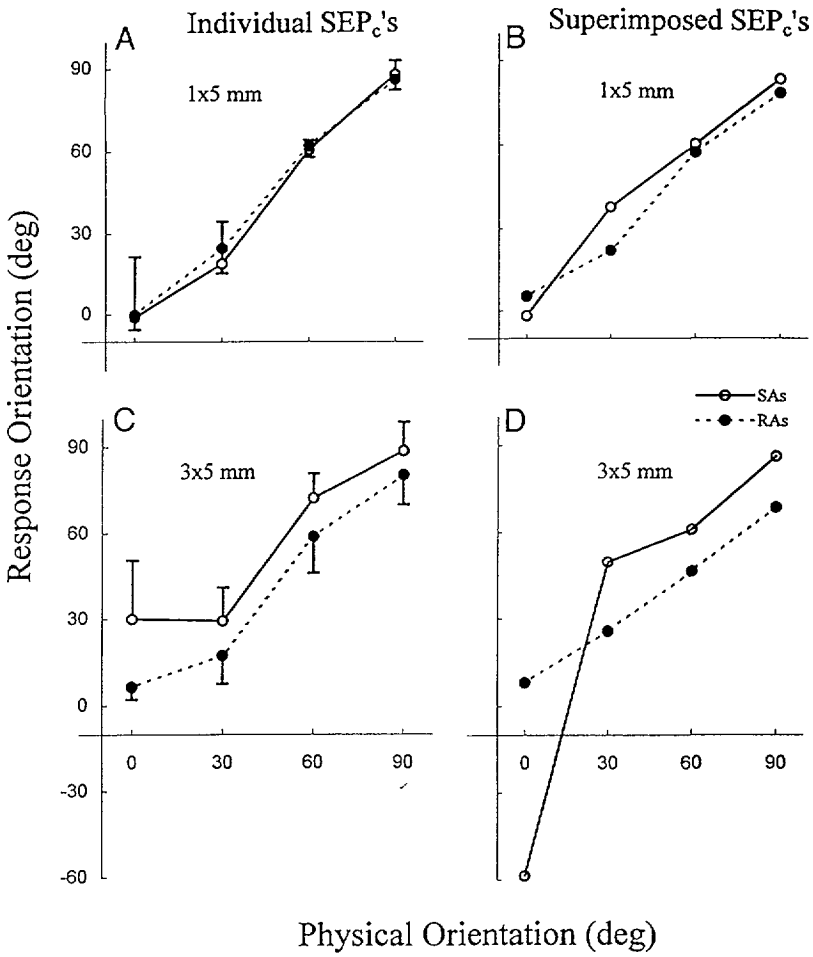

FIG. 7. Relationship between the physical orientation of the major axis of each toroid and the orientation of the major vector obtained from the spatially distributed responses of single fibers or a group of fibers of each type. *A* and *C*: mean major vectors, obtained by principal components analyses of the "individual SEP_cs" evoked in single SAs (——) and RAs (– – –) produced in response to each orientation of the 1 × 5 mm toroid (*A*) and the 3 × 5 mm toroid (*C*). *B* and *D*: major vectors determined for "superimposed SEP_cs," i.e., each combined SEP_c, obtained from the superimposed responses of 6 SAs (——) and 5 RAs (– – –) to each orientation of the 1 × 5 mm toroid (*B*) and the 3 × 5 mm toroid (*D*). Error bars are SEs.

SAs exhibited a singular response of increasing, followed by decreasing, discharge rate that fell well short of the length of the object. In such cases, the distance between the onset of the SA and RA responses and the OFF response of the RAs provided the best indication of the relative spatial extent of the object in the direction of stroking.

NEURAL REPRESENTATIONS OF THE CROSS-SECTIONAL SHAPE OF THE OBJECT IN THE VERTICAL PLANE. The neural representation of the profile of the object's shape in a third dimension was estimated by measuring the SRP along the minor and major axes of the SEP_c of each fiber's response to each object (as described in Fig. 3*B*). The orientations of the object and stroke trajectory were fixed at 90 and 0°, respectively.

SPATIAL RATE PROFILES REPRESENTING THE CROSS-SECTIONAL PROFILE OF EACH OBJECT ALONG THE MINOR AXIS. SRPs obtained from the responses of a typical SA and RA are shown in Fig. 9, *A* and *C*, respectively. The toroid having the greatest curvature on the minor axis evoked the highest discharge rate in each fiber, whereas the sphere elicited the lowest. That is, the mean peak discharge rate increased with increases in object curvature.

The SRPs for each fiber were normalized to the maximal rate, obtained in response to the 1 × 5 mm toroid, and presented in Fig. 9, *B* and *D*. Normalization enabled us to compare the shapes of each SRP independently of differences in height. The circular profile of the object was represented differently in the SRPs of SAs and RAs. The SRP for an SA typically had a single peak and a shape that was approximately triangular with a rounded top. In contrast, the SRP for an RA was typically bimodal, the first portion having a higher peak than the second, corresponding to the ON and OFF phases of the response. The shape of each portion was a little more irregular than that for the SA's response but was approximately triangular in appearance.

The spatial parameters related to the shapes of these normalized profiles were determined by measuring the width of the base of the response to the raised object and the average slopes of the rising and falling portions of the triangular response (see METHODS and Fig. 3*C*). For the RAs, the slopes were determined only for the first, triangular portion of the response and not for the second or OFF phase of the response. The widths of the base of the SA response to the 1 × 5 mm toroid and the width of the base of the first portion of the RA response to the same object were virtually identical at a mean of 2.4 mm (averages for 16 SAs and 11 RAs). The base of the SA response typically decreased with decreases in the width of the object along its minor axis as shown in Fig. 9. The same was true for the entire width of the RA response, although the width of the first portion of the RA response changed little among the three objects. Thus an effect of the decrease in object width was to decrease the separation between the two portions of the RA. At the same time, the increase in object curvature caused an increase in the peak discharge rate.

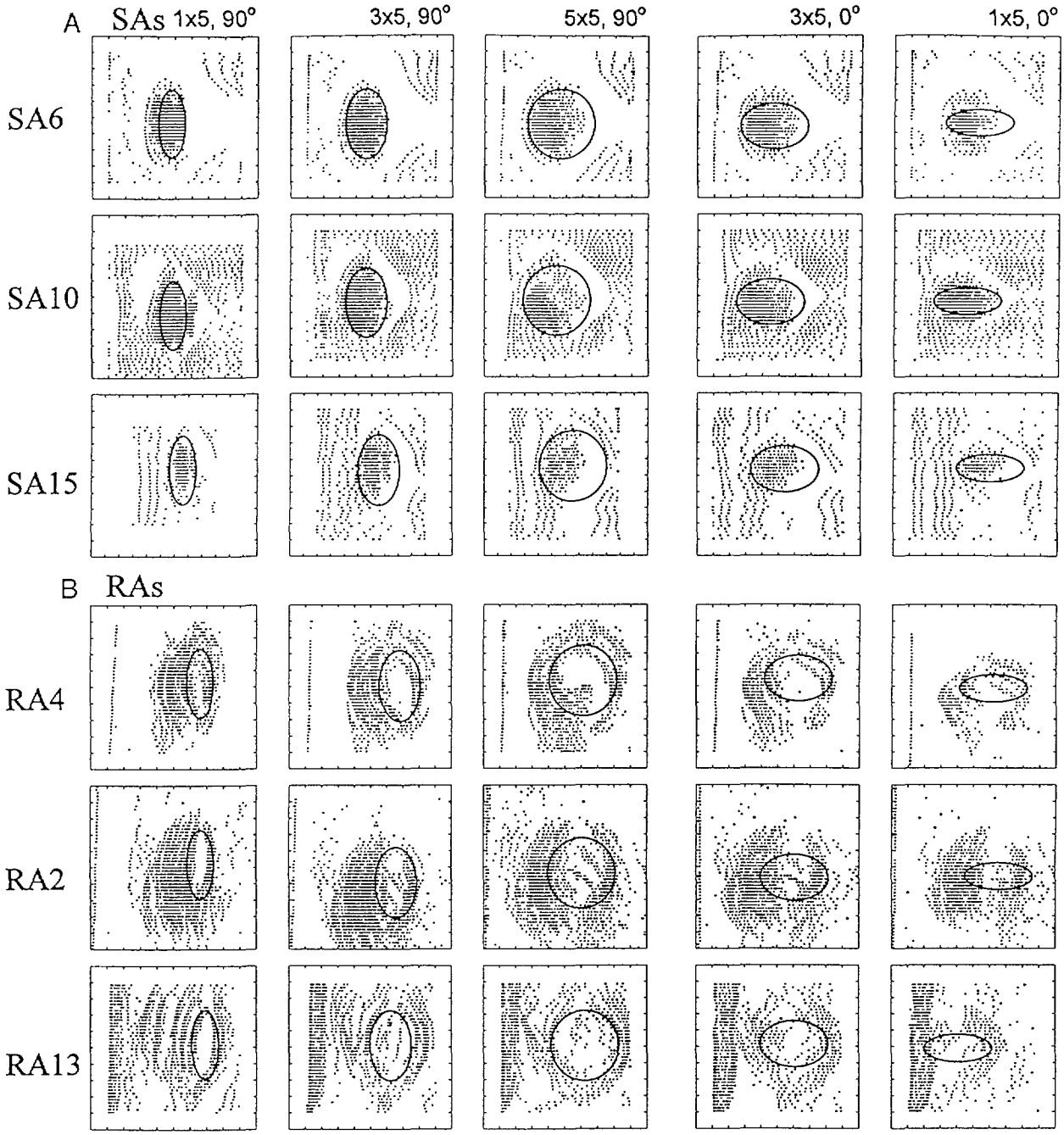

FIG. 8. Comparisons of the outline of the base of each object with the 2-dimensional shape of the SEP evoked by the object in typical SAs and RAs. The SEP in each panel was obtained in response to the object of stated radii (mm) and orientation. The outline of the base of each object on the flat plate is superimposed at an arbitrary position near the leading edge of the response. Spacing between tic marks on each axis is 1 mm. *A*: responses of SAs. *B*: responses of RAs. Each object was stroked from left to right.

Another effect of increases in object curvature along the object's minor axis was to increase the magnitude of the slope of the falling phase of the SRPs for the SAs. This was not only an effect of the corresponding increase in peak discharge rate, because the effect was still present after discharge rate was normalized (Fig. 9*B*). There were less consistent or negligble effects of object curvature on the slopes of the rising phases of the SRPs of the SAs or either rising or falling slopes for the RAs.

The relationships between the size and shape of the object and each response measure (peak height, width, and falling slope of the SRP) were similar for fibers of a given type. To obtain average relations between curvature and each of these measures, independent of differences in fiber sensitivity, each fiber's peak discharge rate to each object was normalized by dividing it by a scaling factor. This factor was obtained for each fiber by dividing its mean peak rate over the three objects by the grand mean peak rate obtained from

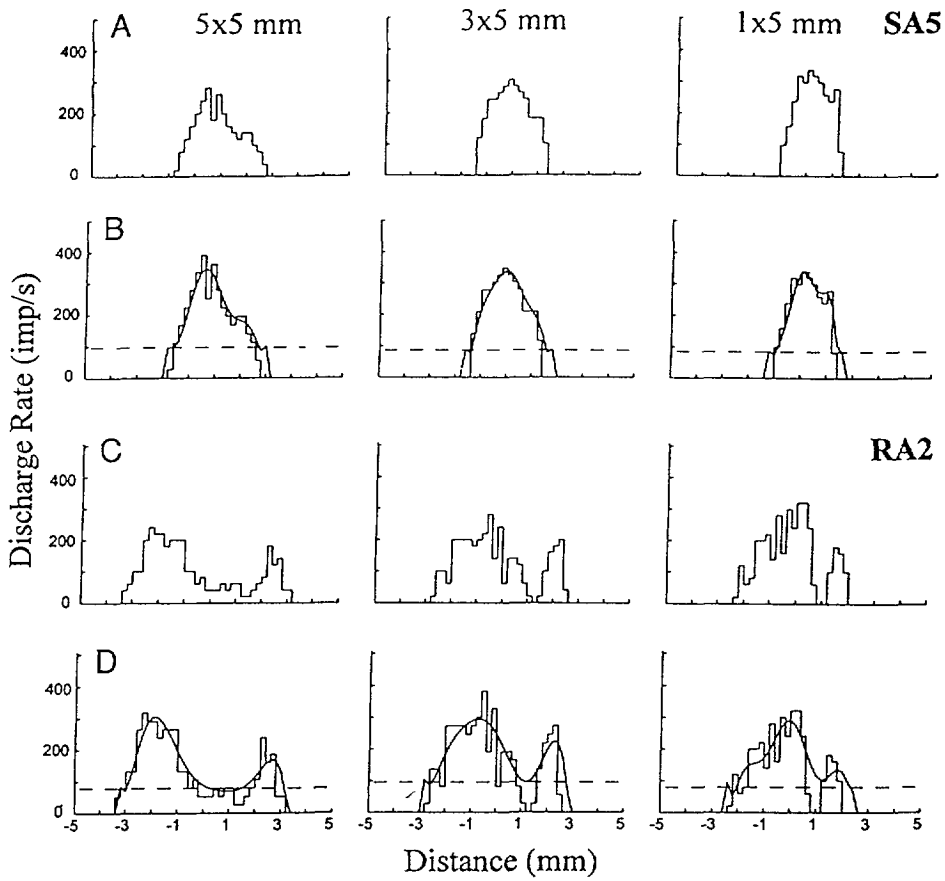

FIG. 9. SRPs representing the middle cross-sectional shape of each object, along the minor axis. *A*: nonnormalized SRPs. Each panel displays the mean spatial discharge rate (impulses/s) along the middle section of the SEP_c, as described in Fig. 3*B*, of the responses of an SA to the sphere, and to the 2 toroids each oriented at 90°. Each object was stroked from left to right. *B*: normalized SRPs. Each SRP in *A* was normalized to the peak discharge rate evoked by the 1 × 5 mm toroid and fitted with a polynomial function. The width of each function along the dashed horizontal line (at 25% of the peak height), and the rising and falling slopes were determined as described in Fig. 3*B*. *C* and *D*: SRPs of an RA displayed in the same format as described for the SA.

all fibers of a given type (SAs or RAs). Thus the scaling factor made the mean peak rate for each fiber equal to the grand mean. For RAs, the heights and slopes were obtained from the rising and falling phases of the ON and not the OFF response, whereas the widths (75% from peak, i.e., along dashed lines in Fig. 9) represent the extent of the entire response. Then the grand mean of the heights, widths, and slopes of the normalized SRPs along the minor axis were obtained from 16 SAs and 11 RAs in response to each object stroked in the forward direction (Fig. 10). For both SAs and RAs there is an apparent trend toward an increasing peak discharge rate, decreased width, and increased falling slope of the SRP with increasing curvature along the minor axis of the object. Repeated measures ANOVAs revealed a significant effect of curvature on the heights (maximal discharge rates) and widths of the SRPs for both SAs and RAs. The same results were obtained in response to strokes in the backward direction. There were no differences in any response measure due to the two directions of stroking. For either direction of stroking, the slope of the falling phase increased significantly with curvature for SAs but not for RAs. A similar trend was found for SAs in the rising phase, although this effect did not reach significance ($P = 0.07$). Curvature had no consistent or significant effects on either rising or falling slopes of the SRP for the RA ON response.

SPATIAL RATE PROFILES REPRESENTING A CROSS-SECTIONAL PROFILE OF EACH OBJECT ALONG THE MAJOR AXIS. The SRPs representing a cross-sectional profile of the object along the major axis (always oriented at 90° to the stroke direction) are shown for the same SA and RA in Fig. 11, *A* and *C*, respectively. The overall shape of the SA's SRP was generally tentlike or triangular with a rounded top. The top portion was sharper for the 1 × 5 mm toroid and a little rounder and broader for the 3 × 5 mm toroid and the sphere (Fig. 11*A*). The overall shape of the RA SRP along the major axis was more rounded and moundlike for the 1 × 5 mm toroid, in comparison with that for the SA (Fig. 11*C*). The shape became flatter and slightly more irregular for the 3 × 5 mm toroid and the sphere. As already mentioned for the SRPs parallel to the minor axis, the mean maximal discharge rate, for SAs and RAs, i.e., the peak height of the SRP, increased with an increase in curvature on the minor axis. To analyze the effect of changes in curvature of the minor axis on the width of the response along the major axis, the SRPs for each SA and RA were normalized to the maximal discharge rate, obtained in response to the 1 × 5 mm toroid (Fig. 11, *B* and *D*). The mean width of the SRPs for all RAs was 1 mm greater than that for all SAs (5.6 vs. 4.6 mm) a difference equal to the difference in the mean length of the von Frey determined receptive field (4.65 vs. 3.64 mm for RAs and SAs, respectively). A repeated measures ANOVA of the widths of the normalized SRPs demonstrated that the differences in object curvature on the minor axis did not produce significant differences in the widths of the SRPs along the major axis for either fiber type and for either direction of stroking. In response to the sphere, the mean widths of the SRPs, parallel to the forward direction of stroking were 4.4 mm for SAs and 5.2 mm for RAs. These values were not

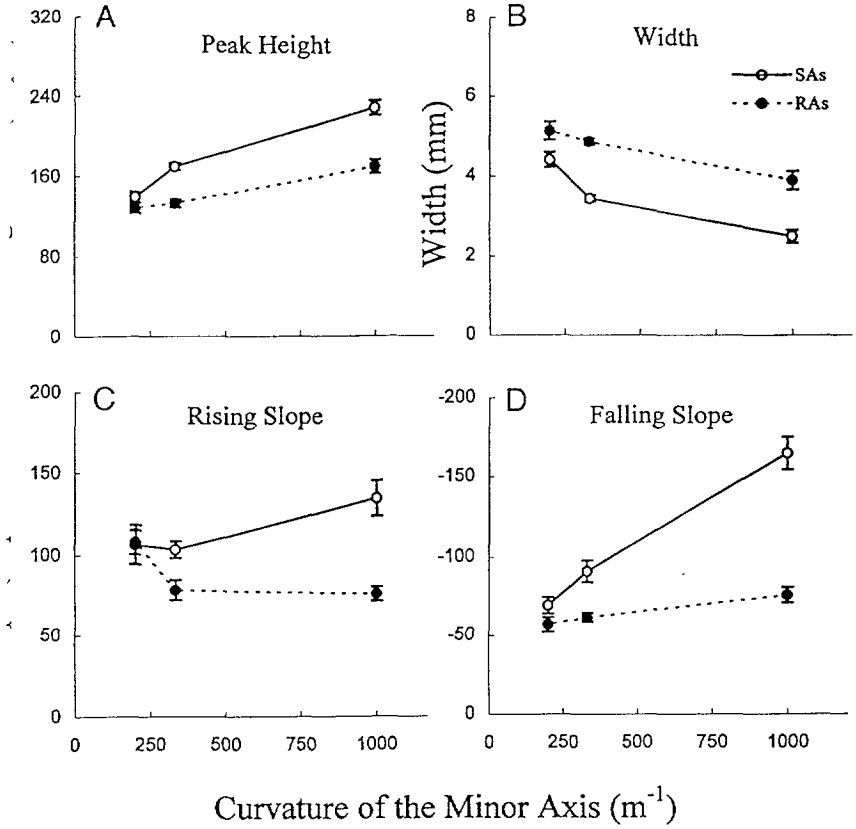

FIG. 10. Peak height, width, and slopes for the rising and falling phases of the middle, cross-sectional SRP along the minor axis. Mean values of each parameter for SAs (——) and RAs (– – –) are plotted as a function of the curvature of the object on the minor axis. The orientation of each toroid was 90°. *A*: mean peak height of the SRP (peak discharge rate). *B*: mean width of the SRP. *C* and *D*: mean slopes of the rising and falling phases of the SRP.

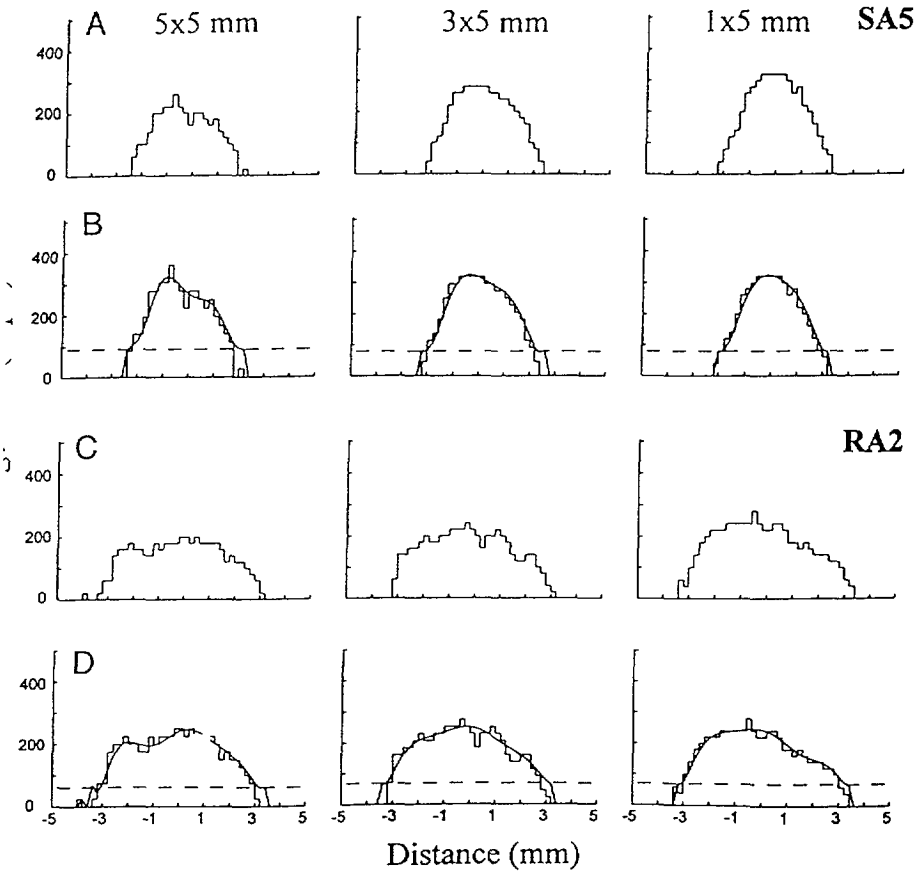

FIG. 11. Spatial rate profiles representing the cross-sectional shape of each object along the major axis. Same format as in Fig. 9.

significantly different from the mean widths of the SRP, orthogonal to the direction of stroking, 4.8 and 5.4 mm, respectively, nor significantly different from the mean SRP widths along the major axes obtained in response to the two toroids (paired *t*-tests). Similar results were obtained for strokes in the backward direction. Thus the size (length) of the major axis of each object is coded consistently in the width of the SRP along the major axis, regardless of changes in the width or curvature of the object along the minor axis.

The mean slope of the falling phase of the minor axis of the SA SRP (−1.24 impulses/s/mm) obtained in response to the sphere, was not significantly different from the mean slope of the falling phase of the major axes obtained for this and the other two objects (−1.2 to −1.3). Thus the constant shape of each object along the major axis was represented in a constant shape of the SA SRP along the major axis. A similar analysis was not reasonable for the RA SRPs due to their bimodal nature for the minor axis and, for the wider objects, their irregular or bimodal shape along the major axis.

NEURAL REPRESENTATIONS OF THE THREE-DIMENSIONAL SHAPE OF THE OBJECT. To obtain a first estimate and overall visual impression of the neural coding of object shape in three dimensions, the responses of each fiber of a given type were combined as follows. The SEP_cs obtained from the responses of each fiber to a given object stroked in the forward direction were aligned by their geometrically determined centers and then superimposed. Next, a matrix composed of areal instantaneous frequencies from each spatial cell (SRS) was obtained from the pooled responses and then smoothed as described in Fig. 3*C, middle*. These are shown for SAs and RAs without normalization both from an oblique view (Fig. 12, *A* and *C*, respectively), and from a frontal view, parallel to the minor axis, after normalization for peak discharge (Fig. 12, *B* and *D*). The shapes of these SRSs are qualitatively similar to most of those obtained, in similar fashion, from individual fibers (e.g., Fig. 3*C, middle*). The representation of the sphere in the SA SRS is approximately conical (with rounded apex). The cone becomes thinner along the minor axis with increasing object curvature, i.e., increasing deviation from sphericity. The representations of shape in the RA SRS are bimodal with the response to the leading edge greater in height than the response to the trailing edge. The heights of each portion of response increase with increasing object curvature and the spacing between the two portions decrease with the corresponding decrease in object width.

The frontal views of the normalized representations of each SRS in Fig. 12, *B* and *D*, illustrate the more important results obtained in the present experiments. First, there is a similarity in the shapes of the SA response profiles, i.e., they are approximately triangular, with rounded tops, and thus not isomorphic with the shape of the object. The implication is that the circularity of the object, i.e., the constant curvature along its major or minor axis, is coded by the approximately constant slope on the rising and falling phases of the corresponding surface of the SA SRS parallel to that axis. The second result is that only the RAs provide information about the location of the trailing edge of the object. Finally, both populations provide information about the relative sizes of the objects by the widths of their responses in the horizontal plane, i.e., parallel to the surface of the skin.

To obtain more quantitative estimates of the neural representation of three-dimensional shape in the population responses of SAs and RAs, the SRSs obtained from the SEP_cs of responses of individual fibers to the sphere and each toroid, oriented at 90°, were each fitted by Gaussian equations (Fig. 3, *C* and *D*, and METHODS). For RAs, only the first, ON portion of the bimodal response was fitted. A Gaussian surface was fitted to the SRS obtained from each fiber's response to each object stroked in each direction as shown for an SA in Fig. 13. The goodness-of-fit and the peak height of the SRS were determined and averages obtained for 16 SAs and 11 RAs. Mean values of goodness-of-fit and Gaussian parameters obtained from the Gaussian fitted SRSs of the 16 SAs when each object was stroked in the forward direction are shown in Table 1. Then the peak height of each SRS for a given fiber was normalized to that obtained in response to the 1 × 5 mm torroid. From cross-sectional profiles through the center of each normalized, Gaussian fitted SRS, parallel to the minor or major axis of the object, the rising and falling slopes and widths at 25% of the distance from base to peak were determined and averages obtained for each axis for each fiber type. The significance of differences in object curvature on each parameter were determined by repeated measures ANOVAs (3 minor-axis curvatures and 2 directions of stroking). Post hoc pairwise comparisons were made with Student-Newman Keuls tests. There was no significant effect of stroke direction on any of the parameters for either SAs or RAs. Mean values of each parameter in Table 2 were obtained from the responses of SAs, averaged for the two directions of stroking (each value representing the mean for 32 samples, i.e., 16 SAs and 2 stroke directions). The mean R^2 values, indicating goodness-of-fits, were significantly higher for SAs than for RAs (2-way repeated measures ANOVA) and significantly higher the greater the object's minor-axis curvature (values for 1 × 5 mm object greater than those for the 3 × 5, which were greater than those for the 5 × 5). For the SAs, there was a significant effect of object curvature on every parameter except rising slopes (minor or major axes) and the width parallel to the major axis. Along the minor axis of the SRS, the peak height and falling slope were significantly greater, and the width smaller the greater the curvature on the minor axis of the object (with all pairwise comparisons significantly different for the 3 curvatures). In contrast, for RAs, there were few significant effects of differences in curvature on each parameter. A notable exception was the mean peak height, which increased significantly as a function of curvature.

Effect of object orientation on neural representations of shape in SA responses

Before obtaining the Gaussian fitted SRS, the coordinates of SEPs obtained for objects whose orientations deviated from 90° were rotated by the amount of the deviation such that the SEP for a 0° orientation was rotated by 90°, the SEP for 30° by 60°, and the SEP for 60° by 30°. Asymmetric Gaussian surfaces were fitted to the SRSs obtained from the nonnormalized responses of six SAs to each orientation of each toroid stroked in each direction. Results obtained from the two stroke directions were averaged. The mean peak height is plotted in Fig. 14*A* as a function of orientation for strokes in the forward direction. The mean peak height

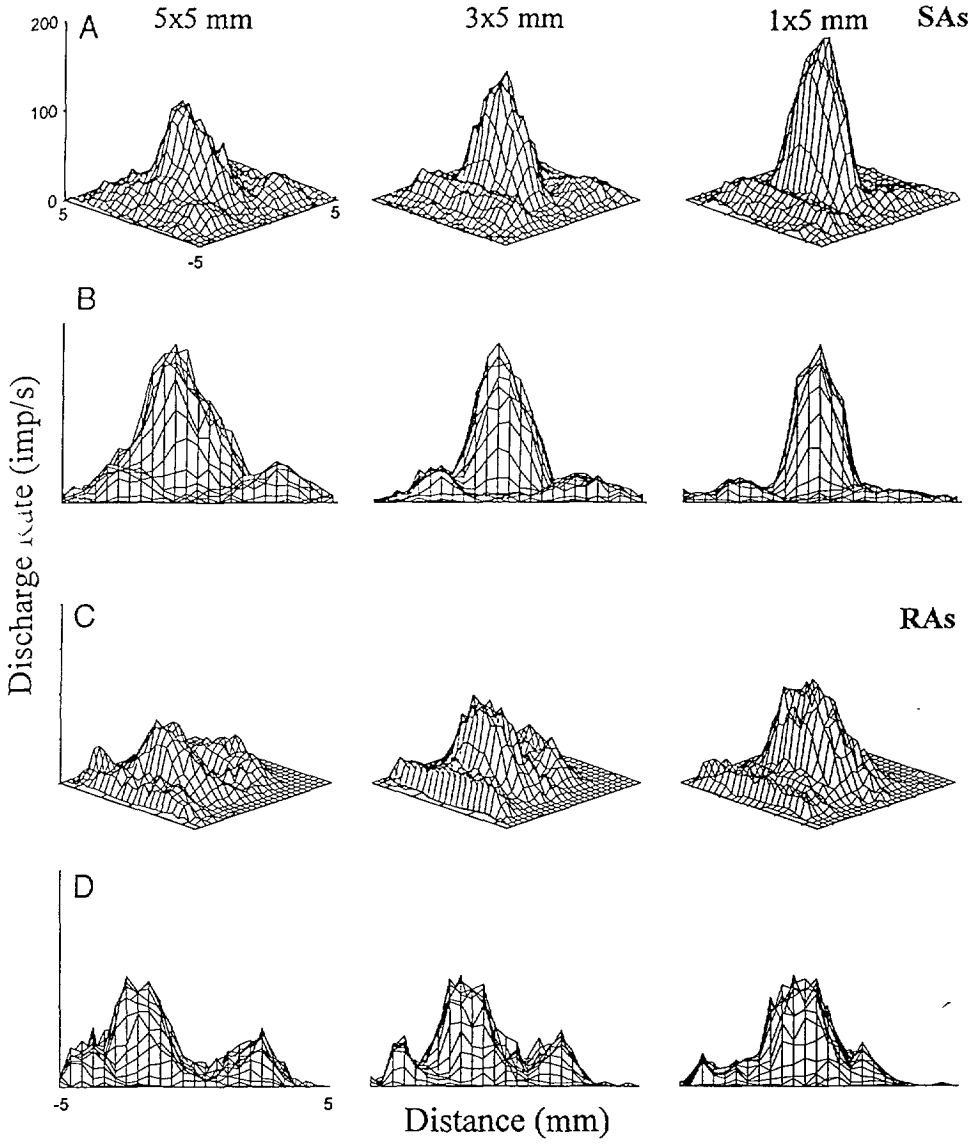

FIG. 12. Smoothed mesh plots of the superimposed spatial discharge rate surfaces obtained from the combined responses of SAs and RAs to each object. *A* and *C*: oblique view of the nonnormalized spatial discharge rate surfaces (SRSs), fitted as described in Fig. 3*C*, *middle*, obtained from the combined responses of 16 SAs (*A*) and 11 RAs (*C*) to each object. The orientation of each toroid was 90°. *B* and *D*: frontal view of the same data as in the panel above, after normalization to the peak discharge rate obtained in response to the 1 × 5 mm toroid.

obtained from the responses of the 5 × 5 mm object at a single orientation (0°) is also shown. Measures of width and slope were then obtained for each SA after normalizing the peak height of each SRS to the greatest peak height obtained. This was always obtained from the response to the 1 × 5 mm toroid oriented at 90°. The mean width, the mean rising slope, and the mean falling slope were each obtained from cross-sectional profile through the Gaussian fitted surface along the minor axis. These are plotted for the sphere at a single orientation and for each toroid as a function of the orientation (Fig. 14).

The effect of orientation on the neural representations of shape in the responses of six SAs was statistically evaluated with two-way repeated measures ANOVAs (shape × orientation) on values for each parameter obtained from the Gaussian fitted SRSs. For each parameter, the ANOVA had two categories of shape (the 2 toroids) and eight categories of orientation (the same 4 orientations for forward and for backward strokes). We did not obtain data for different "orientations" (rotations) of the spherical object. The parameters were peak height, obtained from nonnormalized Gaussian fitted SRSs, and the rising and falling slopes and widths at 25% of the peak of cross-sectional profiles through the centers of normalized Gaussian fitted SRS, parallel to the minor and major axes. The mean peak height increased as a function of increasing orientation from 0 to 90°. There was no significant effect of orientation on either width or slope. The 1 × 5 mm toroid evoked a significantly greater peak discharge rate and a significantly greater width and falling slope than the 3 × 5 mm toroid at all orientations of each object. Rising slopes were not significantly affected by differences in shape or orientation. Thus the neural representations of differences in shape of the toroids, as measured by differences in heights, widths, and falling slopes of SA SRSs, were preserved when the orientation of each object was changed.

A similar analysis of the effects of orientation on shape encoding by RAs was not carried out because, unlike the SAs, they failed to respond to the middle region of the minor axis as the angle between the major axis and the direction of stroking approached zero. That is, although RAs exhibited

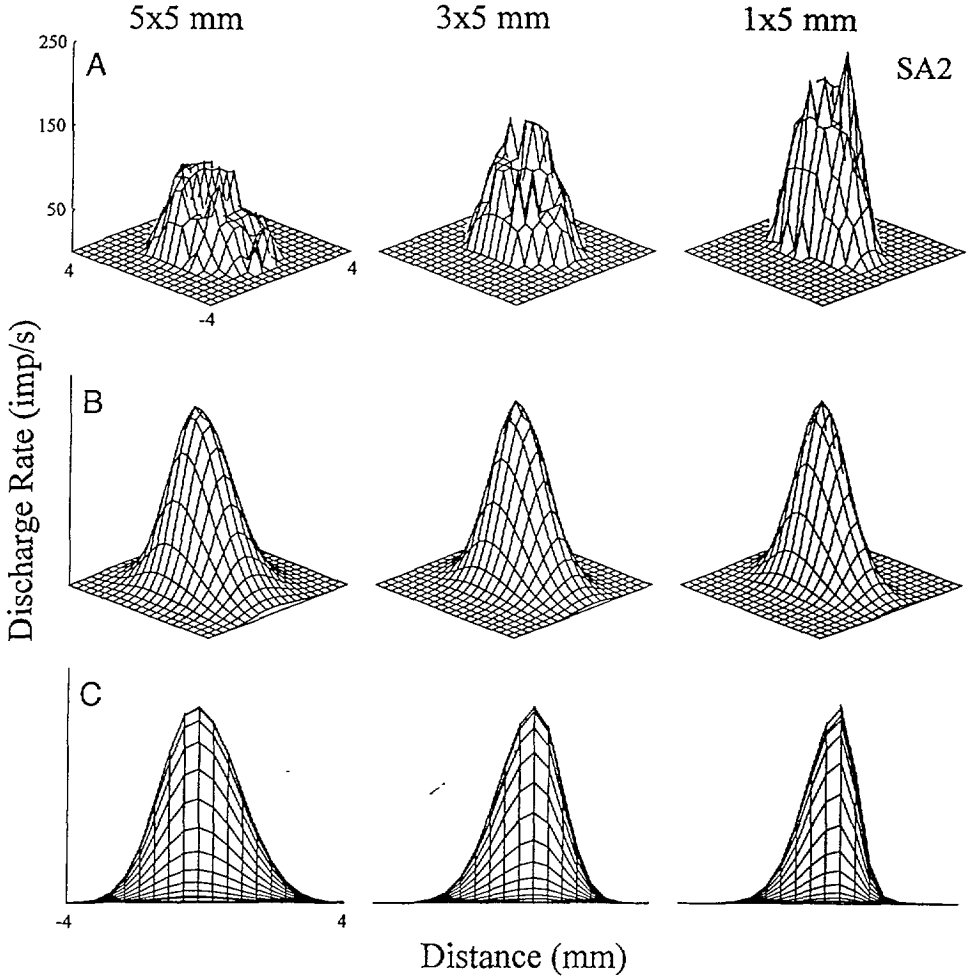

FIG. 13. Mesh plots and Gaussian surface fits of the spatial discharge rate surfaces obtained from the responses of a typical SA to each object. The orientation of each toroid was 90°. *A*: mesh plots of the nonnormalized spatial discharge rate surfaces (SRSs) obtained from the fiber's SEP_ss (refer to Fig. 3*C*, *left*). *B*: Gaussian surface fit of each SRS in *A* after normalization to the peak discharge rate obtained in response to the 1 × 5 mm toroid. *C*: frontal view of the Gaussian surfaces in *B*.

an OFF response that contributed to a coding of orientation, the brevity of their ON responses to longer objects left a gap in response to the middle portion of the object.

DISCUSSION

When actively stroking a stationary object with a fingerpad, multiple sources of information about intended movements and their kinesthetic and cutaneous sensory consequences can be integrated to obtain knowledge of the object's orientation and shape on the skin. The goal of the present experiments was to investigate the sensory coding of the orientation and shape of an object stroked across the fingerpad in the responses of cutaneous afferent fibers. To eliminate information derived from active movement and confine the sensory input to cutaneous receptors alone, methods were developed to stroke objects of differing shape and orientation across the passive fingerpad while controlling the object's contact force and its velocity and direction of movement. It was determined that human observers could readily discriminate the orientations and shapes of the experimental objects regardless of whether the objects were actively explored or presented to the passive fingerpad under stimulus conditions employed in the neurophysiological experiments. Because the attributes of orientation and shape can be independently discriminated by humans via tactile cues alone, we explored candidate mechanisms by which each attribute could be independently coded in the responses of SA and RA afferents to objects stroked across the passive monkey fingerpad.

The orientation or shape of an object in contact with the skin are probably best represented in the spatial distribution of discharges in the responses of a population of cutaneous mechanoreceptors. Such attributes may not be reliably represented in the responses of any single fiber because these

TABLE 1. *Mean values of goodness-of-fit and Gaussian parameters obtained from the Gaussian fitted SRSs of 16 SAs when each object was stroked in the forward direction*

Parameter	Object Curvature on Minor Axis, m^{-1}		
	200	333	1,000
R^2	0.62	0.70	0.74
Peak height (a), imp/s*	84	106	156
x_r width (c), mm†	0.92	0.80	0.75
x_f width (d), mm	1.38	1.01	0.69
y_r width (f), mm	1.31	1.27	1.27
y_f width (g), mm	1.47	1.34	1.34

The orientation of each toroid was 90°. * Mean peak heights are from nonnormalized SRSs, whereas the widths are from SRSs that were normalized to each SA's greatest peak response (i.e., to the object with a minor axis of 1,000 m^{-1}). † Mean widths (c–g) of the Gaussian surface at 60.7% of the peak height for the rising (r) and falling (f) segments of the surface along the x (minor) and y (major) axes.

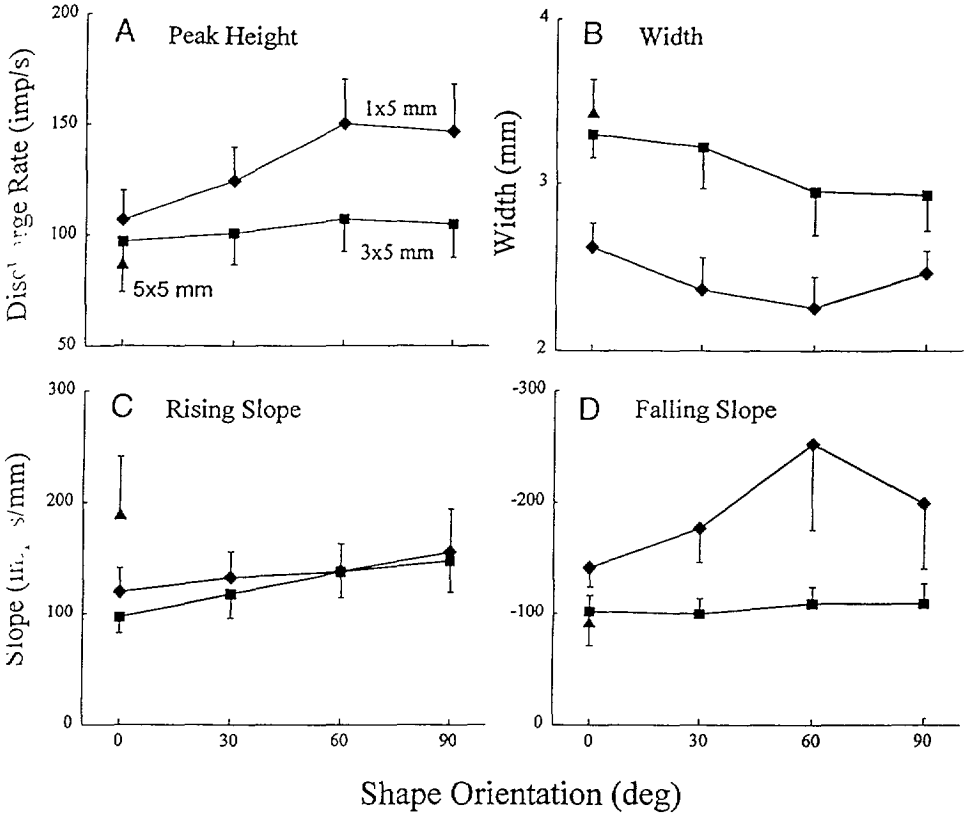

FIG. 14. Effects of changes in object orientation on the mean peak height, mean width, and mean slopes obtained from Gaussian surface fits of the SA spatial discharge rate surfaces (SRSs) obtained in response to objects of differing curvature. Radii of curvature are given in mm. The means were obtained from the SRSs of 6 SAs. *A–D*: results for height, width, rising slopes, and falling slopes, respectively.

esponses may be confounded by an object's size and how t is applied to the skin, for example, its contact force, velocty, and direction of translation (e.g., Goodwin et al. 1995; aMotte and Srinivasan 1987a,b; Srinivasan and LaMotte 987). An intensive response measure such as peak discharge rate, which we found can reflect differences in shape r in orientation when other stimulus parameters are held onstant, is predicted to be less robust than spatial measures such as width and slope obtained from the responses of a population of fibers.

ABLE 2. *Mean slope and mean width measures derived from ross-sectional profiles along the minor and major axes of aussian-fitted SRSs of 16 SAs*

Parameter	Object Curvature on Minor Axis, m^{-1}		
	200	333	1,000
inor axis			
Rising slope,* imp/s/mm	170	176	181
Falling slope, imp/s/mm	86	111	188
Width,† 25% peak, mm	3.84	3.02	2.39
ajor axis			
Rising slope, imp/s/mm	91	87	85
Falling slope, imp/s/mm	75	84	79
Width, 25% peak, mm*	4.64	4.35	4.34

Each mean in the table was obtained by averaging the values obtained r forward and backward stroke directions for 16 SAs. The orientation of ch toroid was 90°. SRSs, spatial discharge rate surfaces; SAs, slowly apting, type I mechanoreceptive afferents. * Each slope measure is the ing or falling slope of a line connecting points on the Gaussian profile cated, respectively, at heights of 25 and 75% from the peak. † Each width easure is the mean length of a horizontal line located 25% of the distance m base to peak and intersecting with rising and falling phases of the ussian profile along the major or minor axis.

A population response to an object can be estimated in different ways. One approach is to apply the object to a given locus on the skin and record the responses of an actual, representative population of mechanoreceptors with receptive fields distributed across the skin. This is the method we recently used to investigate coding of the shapes and orientations of full-sized versions of the objects used in the present study as they were statically indented (Khalsa et al. 1998). Another approach, the one taken in the present experiments, is to estimate the population responses from the responses of single mechanoreceptive afferent fibers to different locations of the object with respect to the centers of their receptive fields. An estimation of the spatial distribution of neural activity, parallel to the surface of the skin, is obtained in the spatial event plot of the location of the object at each occurrence of an action potential. The two-dimensional shape and orientation of any part or all of this "surface parallel" distribution of activity (the SEP) can be interpreted as encoding the outline of the size, shape, and orientation of the corresponding portion of the object in contact with the skin (e.g., Goodwin et al. 1989; Johnson and Lamb 1981; LaMotte and Srinivasan 1987a,b, 1996; Phillips and Johnson 1981). The shape of a spatial discharge rate surface (SRS) obtained from these data not only contributes to orientation coding but also represents a third dimension of object shape, orthogonal to the surface of the skin (Goodwin et al. 1995; LaMotte et al. 1994, 1996). A vertical, cross-sectional profile or slice through this spatial distribution of discharge rates (SRP) is dominantly affected by the vertical cross-sectional shape of the object (Goodwin et al. 1995; LaMotte and Srinivasan 1996).

The present study describes cutaneous spatial mechanisms

for identifying the relative orientation and shape of an object on the surface of the fingerpad. For a raised object on a planar surface, it was shown that a central rate thresholding process would be sufficient to eliminate background discharges evoked by the surround, leaving the two-dimensional "footprint" (the SEP_c) of neural activity in a spatially distributed population of SAs and RAs. The shape of the leading border of the area of neural activity was an approximately isomorphic outline of the contour of the leading edge of the object in contact with, and parallel to, the surface of the skin. It was shown that the distribution of neural activity within the SEP_c, which we interpret as representing a snapshot of the activity of a population of mechanoreceptors, could be used to generate not only a major vector that accurately described the orientation of the toroidal object parallel to the surface of the skin but also to provide a representation of the shape of the object in a third dimension, vertical to the surface of the skin.

Neural coding of orientation

The relative contribution of SA and RA population responses to encoding the orientation of an object differs according to whether the object is stroked across or statically indented into the skin. For static indentation, SAs and not RAs encode the orientation of a toroid (Khalsa et al. 1998) or differences in the orientation of a cylinder (Dodson et al. 1998). For stroking, both SAs and RAs contribute to orientation coding. In the present study, the orientation of the major vector obtained from the estimated population responses (SEP_cs) of SAs and RAs was found to be linearly related to the physical orientation of each toroidal object. This neural representation of the orientation of the major axis of curvature of an object stroked over the skin was also influenced both by the curvature of the object on the minor axis and by the orientation of the stroke trajectory. Clearly, when the object is more asymmetric, that is the greater the difference between its principal curvatures, its orientation on the skin should be more discernible. Our findings are consistent with this a priori prediction in that the neural representation of object orientation in the spatially distributed discharge rates of SAs and RAs was more variable for the 3 × 5 than the 1 × 5 mm toroid. Similarly, it was previously shown that the human capacity to identify a toroidal object's orientation becomes less accurate as the toroids become less asymmetric and more spherical (LaMotte et al. 1992).

The orientation of the stroke trajectory also influenced the neural coding of object orientation on the skin. Because the orientation of the stroke trajectory was held constant in the present study at 0°, i.e., orthogonal to the long axis of the finger, the effect of changes in the orientation of a toroid on the discharge rates of cutaneous afferent fibers was confounded to some extent by concomittant changes in the magnitude and rate of change in the curvature of the skin produced by the laterally moving object. Previous studies found that changes in the magnitude of curvature primarily influence the discharge rates of SAs and not RAs, whereas changes in curvature rate affect the discharge rates of both fiber types (LaMotte and Srinivasan 1987a,b; Srinivasan and LaMotte 1987). The length of skin experiencing a change in skin curvature and the magnitude and rate of change in curvature will be greater when the major axis of an object is orthogonal as opposed to parallel to the direction of stroking. These facts explain why the discharge rates of both SAs and RAs decreased and the shapes of their spatial distribution (SEP_cs) in the horizontal plane became less asymmetric, i.e., more circular as the orientation of the major axis of each toroid was decreased from 90 to 0°. One might suppose that the shapes of the von Frey determined receptive fields, which were ~1 mm longer along the long axis of the finger than they were along the orthogonal axis, might have contributed to the decrease in asymmetry. However, a similar loss of asymmetry was observed in more circular receptive-field shapes. Another possible contribution to decreased asymmetry may result from the approximately cylindrical shape of the finger that is bound to influence the mechanics of contact and the mechanical state at receptor locations in the skin. However, the orientations of the major vectors of the spatially distributed responses of RAs and SAs were not determined solely by the shapes of the outline of activity in the horizontal plane but were also influenced by the spatial distribution of discharge rates within the active region. For example, the asymmetric shape in response outline might have sufficed in coding all orientations of the 1 × 5 mm toroid, whereas an asymmetric distribution of discharge rates within a more spherical outline was required for orientations of the 3 × 5 mm toroid. In any case, despite the spatial and intensive changes in discharge rate that occurred due in part to changes in skin curvature and its rate as object orientation was varied, the orientation of the principal component of the spatially distributed discharge rates in the activated RA and SA population was approximately linearly related to the physical orientation of the object.

RAs were slightly better than SAs in representing certain differences in orientation primarily because of their capacities to respond earlier to the onset of the leading portion of the raised object and also to the offset of the trailing portion. It is well-known that, although both RAs and SAs respond to the onset of an indentation of the skin, only RAs respond during retraction (Knibestol 1973; Pubols 1980; Talbot et al. 1968). RAs are poorer than SAs in coding the shapes of two-dimensional objects stroked across the skin (e.g., Johnson and Lamb 1981; LaMotte and Srinivasan 1987a,b). As shown in the present study, although RAs are poorer than SAs in coding the shapes of curved three-dimensional objects moving over the skin, they are superior in demarcating the locations of the trailing portions of the wider objects in addition to their anticipatory demarcations of the leading portions. This provided a longer spatial rate profile, and thus a slightly more accurate response orientation to a toroidal object as the orientation of the major axis of the object approached zero. The outline of this profile in the horizontal plane became a less important determinant of response orientation, and the spatial distribution of discharge rate became more important as the asymmetry in the outline's shape decreased with diminishing differences between major and minor principal curvatures of the object.

Neural coding of two-dimensional shape parallel to the skin surface

Surface-parallel, spatial neural codes, based on responses of single fibers, have been proposed for discriminations of

two-dimensional, raised patterns, such as Braille-sized raised letters, dots, and gratings stepped or stroked across the fingerpad of human (Phillips et al. 1990) and/or monkey (e.g., Johnson and Lamb 1981; Lamb 1983; Phillips and Johnson 1981). Isomorphic representations of each pattern were present in the responses of SAs and less accurately in responses of RAs but not those of pacinians or type II SAs. Recently, intensive, modal, and temporal neural codes were ruled out in favor of a spatial code for the roughness of embossed dots of varying dot diameter and spacing (Connor et al. 1990; Connor and Johnson 1992). The elements of the patterns in these studies had sharp edges and flat tops. For a given raised element, the transition from a flat surface to leading and trailing edges of high curvature provided an isomorphic image of the spatial extent of the raised element in the direction of stroking. The difference in magnitude of response between leading and trailing edges can be explained as due to a higher reaction force and rate of skin displacement by the leading edge (Blake et al. 1997).

In contrast, the raised objects used in the present study did not have flat tops but were composed of two constant principal curvatures. Consequently, the responses of SAs to the leading and trailing edges of objects were not spatially separated but, instead, were blended into a single response of rising and falling discharge rates. The RAs exhibited a similar, although more irregular, ON response, that appeared to begin earlier than that of the SAs, followed by a second, OFF response that indicated the retraction of the skin as the raised portion moved away from the most sensitive portion of the receptive field. The OFF response serves as a temporal cue indicating the presence of a falling edge as opposed to a continuation of the raised portion of the object. For example, such an OFF response was not present in the responses of RAs to a raised step having a similar curvature (LaMotte and Srinivasan 1987b).

The outlines of the leading edge of the toroidal or spherical object in the horizontal plane and in the direction of stroking were well represented in the leading edge of the SA SEP_cs and, to a lesser extent, those of the RAs. The trailing edge of the object was similarly represented in the trailing edge of the SA SEP_c but less accurately. However, the shape of the region of neural activity in the RA or SA population, hypothesized to be represented by the shape of the SEP_c, was not consistently isomorphic to the shape of the base of the object. The SEP_cs of the RAs were too large and irregular, and those of the SAs had widths that were too short when the length of the object in the stroke direction was larger than 3 or 4 mm. However, it is possible that in the latter case, the shape of the outline of the object-evoked activity in the SA population was approximately isomorphic to the shape of the contact area between the object and the skin.

Neural coding of two- and three-dimensional shape vertical to the skin surface

The shape of the spatial distribution of discharge rates of an estimated population of mechanoreceptors is an estimation of the geometry of an object in a third dimension, orthogonal to the surface of the skin. This representation is not isomorphic to the shape of the object. The raised spherical object was represented in the estimated SA population response as a cone with rounded apex and the toroid as a similar but elongated cone. Similar shapes were obtained in response to spherical objects of different curvature statically indented into the skin (Goodwin et al. 1995). A broadsided or a frontal view of the SA SRS (Fig. 12) reveals an approximately triangular shape as does the SRP representing the two-dimensional cross-sectional profile of the object along the major or minor axes. A sequence of triangular shapes was evoked in the SRP obtained for SAs in response to a wavy surface, consisting of cylindrically shaped surfaces of differing curvature, stroked across the fingerpad (LaMotte and Srinivasan 1996). The width of the base of the triangular shape, normalized for peak discharge (height), decreased with increasing curvature of the cylinder. Similarly, the convex, cylindrically shaped portion of a half-sinusoid step evoked a triangular-shaped SRP, whose base decreased as the wavelength or width of the steps was varied from gradual to steep (LaMotte and Srinivasan 1987a). It was hypothesized that the shape of each circular (cylindrical) object, defined by its constant curvature, was coded in the constancy of the slopes along the rising and declining phases of the corresponding triangular shape in the SRP. The size, or width, of the circular structure was coded in the width of the base of the triangle (LaMotte and Srinivasan 1996).

The results of the present study confirm these hypotheses for the raised, spherical, and toroidal objects on a planar surface. When the minor axis of the object was oriented parallel to the direction of stroking, the SA SRP had a triangular shape whose base decreased with increasing curvature of the minor axis. However, unlike the triangular SRPs evoked in SAs by the wavy surface, those produced by the raised objects were often slightly asymmetric, owing to the fact that the rising phase changed less with curvature than the falling phase. The abrupt change in depth of indentation, to which SAs are sensitive, may have masked the responses to the initial changes in curvature for many SAs.

SKIN-CURVATURE HYPOTHESIS. With the use of a model proposed earlier (LaMotte and Srinivasan 1987a,b; Srinivasan and LaMotte 1987, 1991), it is possible to relate the shape of the raised object to the probable profile of skin deflection and the responses of each type of mechanoreceptor. It is hypothesized that SA responses are governed by not only the depth and velocity of indentation of the skin, but also the rate and amount of a positive change in the curvature of the skin at the most sensitive spot in the receptive field. RAs are primarily responsive to changes in the velocity of the skin at the most sensitive spot and the rate of change in the curvature of the skin. A change in skin curvature from its normally convex position to one more concave (as occurs during indentation) is defined as a positive change, whereas an increase in convexity is defined as negative. The planar surface produces an indentation with a small, positive change in skin curvature, resulting in a basal discharge in the SA. As the raised object approaches the most sensitive spot, before the skin contacts the object, the skin is lifted away from the plate, and there is then a negative change in curvature that can produce a pause in firing. The abrupt change in depth of indentation, together with a positive change in curvature, produces the rising phase of the SA's discharge as the raised object moves onto the most sensitive spot. This is followed

by the effects of a reduced depth of indentation under the trailing half of the object and a negative change in curvature as the curved object continues to move over this most sensitive spot. RAs respond with a burst due to skin stretch caused by horizontal velocity as the planar surface begins its lateral translation and then a response to the negative vertical velocity of local skin retraction as the skin is lifted away from the most sensitive spot in front of the approaching object. This is followed by a response to the positive velocity of indentation by the object that ceases as the velocity approaches zero near the apex of the object. Another response is evoked by the negative velocity produced by the withdrawal of the object relative to the skin near the trailing edge. We are uncertain as to the extent to which curvature rate sensitivity contributes to these responses. However, it seems that the SRPs of the RAs appear to outline the spatial locations and velocities of the indentations and retractions of skin surrounding the object rather than provide an outline of the shape itself in the vertical plane. In contrast, the SAs provide a consistent spatial rate distribution that represents a third dimension of shape in addition to the outline of the shape in contact with the skin in the other two dimensions.

Effects of orientation on neural coding of shape

It is common experience that the shape and size of an object, perceived through the sense of touch, remain generally constant despite changes in its orientation on the skin. The present findings suggest that it is the constancy in the differences in the widths and falling slopes of the SRS and SRPs evoked in the SA population by different raised objects that encodes the constancy of their sizes and shapes regardless of differences in their orientation with respect to the direction of stroking. In contrast, the spatial responses of the RAs provide less reliable measures of shape, owing in part to the brevity of their responses to the onset of curvature and their responsiveness to skin movement produced by the effects of a moving object on the movement of the skin surrounding the object as opposed to the shape of the object. However, such responses provide a kind of negative image or shadow of the object's shape, the onset of which provides a preview of what is to be coded in the responses of the SAs.

The authors thank K. Greenquist and A. Klusch-Petersen for technical assistance.

This work was supported by National Institute of Neurological Disorders and Stroke Grant NS-15888 and Office of Naval Research Grant N00014-91-J-1566.

Address for reprint requests: R. H. LaMotte, Dept. of Anesthesiology, Yale University School of Medicine, 333 Cedar St., New Haven, CT 06510.

Received 8 October 1997; accepted in final form 16 July 1998.

REFERENCES

BLAKE, D. T., JOHNSON, K. O., AND HSIAO, S. S. Slowly and rapidly adapting mechanoreceptive responses to raised and depressed scanned patterns: effects of width, height, orientation, and a raised surround. *J. Neurophysiol.* 78: 2503–2517, 1997.

CONNOR, C. E., HSIAO, S. S., PHILLIPS, J. R., AND JOHNSON, K. O. Tactile roughness: neural codes that account for psychophysical magnitude estimates. *J. Neurosci.* 10: 3823–3836, 1990.

CONNOR, C. E. AND JOHNSON, K. O. Neural coding of tactile texture: comparisons of spatial and temporal mechanisms for roughness perception. *J. Neurosci.* 12: 3414–3426, 1992.

GOODWIN, A. W., BROWNING, A. S., AND WHEAT, H. E. Representation of curved surfaces in responses of mechanoreceptive afferent fibers innervating the monkey's fingerpad. *J. Neurosci.* 15: 798–810, 1995.

GOODWIN, A. W., JOHN, K. T., SATHIAN, K., AND DARIAN-SMITH, I. Spatial and temporal factors determining afferent fiber responses to a grating moving sinusoidally over the monkey's fingerpad. *J. Neurosci.* 9: 1280–1293, 1989.

JOHNSON, K. O. AND HSIAO, S. S. Neural Mechanisms of Tactual Form and Perception. *Annu. Rev. Neurosci.* 15: 227–250, 1992.

JOHNSON, K. O. AND LAMB, G. D. Neural mechanisms of spatial tactile discrimination: neural patterns evoked by Braille-like dot patterns in the monkey. *J. Physiol. (Lond.)* 310: 117–144, 1981.

KHALSA, P. S., FRIEDMAN, R. M., SRINIVASAN, M. A., AND LAMOTTE, R. H. Encoding of shape and orientation of objects indented into the monkey fingerpad by populations of slowly and rapidly adapting mechanoreceptors. *J. Neurophysiol.* 79: 3238–3251, 1998.

KNIBESTOL, M. Stimulus-response functions of rapidly adapting mechanoreceptors in the human glabrous skin area. *J. Physiol. (Lond.)* 232: 427–452, 1973.

LAMOTTE, R. H., LU, C., AND SRINIVASAN, M. A. Tactile neural codes for the shapes and orientations of objects. In: *Somesthesis and the Neurobiology of the Somatosensory Cortex,* edited by O. Franzen, R. Johansson, and L. Terenius. Basel: Birkhauser Verlag, 1996, p. 113–122.

LAMOTTE, R. H. AND SRINIVASAN, M. A. Tactile discrimination of shape: responses of slowly adapting mechanoreceptive afferents to a step stroked across the monkey fingerpad. *J. Neurosci.* 7: 1655–1671, 1987a.

LAMOTTE, R. H. AND SRINIVASAN, M. A. Tactile discrimination of shape: responses of rapidly adapting mechanoreceptive afferents to a step stroked across the monkey fingerpad. *J. Neurosci.* 7: 1672–1681, 1987b.

LAMOTTE, R. H. AND SRINIVASAN, M. A. Responses of cutaneous mechanoreceptors to the shape of objects applied to the primate fingerpad. *Acta Psychol.* 84: 41–51, 1993.

LAMOTTE, R. H. AND SRINIVASAN, M. A. Neural encoding of shape: responses of cutaneous mechanoreceptors to wavy surfaces stroked across the monkey fingerpad. *J. Neurophysiol.* 76: 3787–3797, 1996.

LAMOTTE, R. H., SRINIVASAN, M. A., AND KLUSCH-PETERSEN, A. Tactile discrimination and identification of the shapes and orientations of ellipsoidal objects. *Soc. Neurosci. Abstr.* 18: 830, 1992.

LAMOTTE, R. H., SRINIVASAN, M. A., LU, C., AND PETERSEN, A. K. Cutaneous neural codes for shape. *Can. J. Physiol. Pharmacol.* 72: 498–505, 1994.

LAMOTTE, R. H. AND WHITEHOUSE, J. Tactile detection of a dot on a smooth surface. *J. Neurophysiol.* 56: 1109–1128, 1986.

LAMB, G. D. Tactile discrimination of textured surfaces: peripheral neural coding in the monkey. *J. Physiol. (Lond.)* 338: 567–587, 1983.

MORRISON, D. F. The structure of multivariate observations. I. Principal components. In: *Multivariate Statistical Methods.* New York: McGraw-Hill, 1967, p. 221–258.

PHILLIPS, J. R., JOHANSSON, R. S., AND JOHNSON, K. O. Representation of Braille characters in human nerve fibers. *Exp. Brain Res.* 81: 589–592, 1990.

PHILLIPS, J. R. AND JOHNSON, K. O. Tactile spatial resolution. II. Neural representation of bars, edges and gratings in monkey primary afferents. *J. Neurophysiol.* 46: 1192–1203, 1981.

PUBOLS, B. H. ON- versus OFF-responses of raccoon glabrous skin rapidly adapting cutaneous mechanoreceptors. *J. Neurophysiol.* 43: 1558–1570, 1980.

SRINIVASAN, M. A. AND LAMOTTE, R. H. Tactile discrimination of shape: responses of slowly and rapidly adapting mechanoreceptive afferents to a step indented into the monkey fingerpad. *J. Neurosci.* 7: 1682–1697, 1987.

SRINIVASAN, M. A. AND LAMOTTE, R. H. Encoding of shape in the responses of cutaneous mechanoreceptors. In: *Information Processing in the Somatosensory System,* edited by O. Franzen and J. Westman. London MacMillan, 1991, p. 59–69.

TALBOT, W. H., DARIAN-SMITH, I., KORNHUBER, H. H., AND MOUNTCASTLE, V. B. The sense of flutter-vibration: comparison of the human capacity with response patterns of mechanoreceptive afferents from the monkey hand. *J. Neurophysiol.* 31: 301–355, 1968.